Special Issue Papers

Polarization and Spatial Information Recovery by Modal Dispersal and Phase Conjugation: Properties and Applications

YASUO TOMITA, MEMBER, IEEE, RAM YAHALOM, KAZUO KYUMA, MEMBER, IEEE, AMNON YARIV, FELLOW, IEEE, AND NORMAN SZE-KEUNG KWONG, MEMBER, IEEE

(Invited Paper)

Abstract—**We describe recent theoretical and experimental studies of polarization and spatial information recovery by modal dispersal and phase conjugation. We discuss the fidelity of this phase-conjugation process as a function of input-beam launching conditions. We also describe several new applications of the scheme which involve correction of nonreciprocal polarization distortions, correction of lossy amplitude distortions, phase-conjugate multimode fiber-optic interferometers and gyros, temporal data channeling between beams, and all-optical beam thresholding.**

I. INTRODUCTION

OPTICAL phase conjugation has been investigated extensively in many areas of nonlinear optics [1]. In particular it is well known that it can be used to correct *phase* distortions because of the wavefront-reversal properties of an incoming optical wave. For this reason the main emphasis has been on the study of the properties of *ordinary* phase-conjugate mirrors (PCM's) that reflect waves of a particular polarization (usually a linear polarization). In spite of the usefulness of the ordinary PCM's, however, they cannot be applied to the cases where the distortions include optical anisotropies by which incident waves suffer from *polarization* scrambling as well as phase distortions. This is caused, for example, by the induced birefringence in high power (e.g., Nd-doped glass) optical amplifier stages, and by the strong intermodal coupling in multimode fibers. These call for phase conjugation of both polarization components of the beam.

Manuscript received January 29, 1988; revised June 2, 1988. This work was supported by the U.S. Air Force Office of Scientific Research and the U.S. Army Research Office, Durham, NC.

Y. Tomita, R. Yahalom, and A. Yariv are with the Department of Applied Physics, California Institute of Technology, Pasadena, CA 91125.

K. Kyuma was on leave at the Department of Applied Physics, California Institute of Technology, Pasadena, CA 91125. He is now with the Central Research Laboratory, Mitsubishi Electric Corp., Amagasaki, Hyogo 661, Japan.

N. S.-K. Kwong is with the Ortel Corp., Alhambra, CA 91803.

IEEE Log Number 8825880.

In the late 1970's researchers in the Soviet Union studied both theoretically and experimentally the possibilities of complete polarization and spatial wavefront reversal in stimulated Brillouin scattering (SBS) [2]–[5], degenerate four-wave mixing (DFWM) [6], and stimulated scattering of the Rayleigh line wing [7], for correcting wavefront and polarization distortions caused in high power optical amplifier stages. They found that the complete reversal of an *arbitrary* polarized wave can be achieved by means of the tensorial property of the phase-conjugation process via DFWM, whereas the usefulness of the above stimulated scattering processes is limited to the reversal of depolarized pump waves [8]. Subsequently the experimental demonstrations of complete reversal were conducted using DFWM in liquid CS_2 [9], [10], Nd-doped glass [11], sodium vapor [12], and biochrome films [13]. Phase conjugation using self-pumped photorefractive PCM's [14], [15] was also used for the complete reversal of an arbitrary polarized wave [16]. In this method, which is similar to Basov's scheme [5], an arbitrary polarized incident wave is decomposed into two orthogonally linear polarized components. The polarization of one of the two is rotated by 90° and the two components, now similarly polarized, are then reflected by a single self-pumped photorefractive PCM [17], and their phase-conjugated waves are coherently recombined into one wave. Consequently this method results in the complete reversal (i.e., scalar phase conjugation [18]), provided that the phase-conjugate reflectivities of these two components are exactly equal both in amplitude and phase.

A new and fundamentally different scheme for scalar phase conjugation was reported by Kyuma *et al.* [19]. This scheme, which consists simply of a tandem combination of a multimode fiber and a self-pumped photorefractive PCM (see also Fig. 1), uses the inherent strong intermodal coupling (i.e., modal dispersal) in the fiber combined with phase conjugation of *one* polarization com-

0018-9197/89/0300-0315$01.00

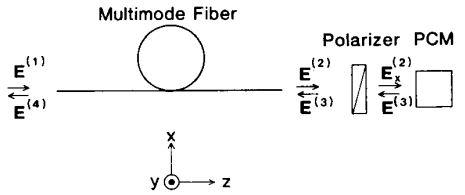

Fig. 1. Schematic diagram of the fiber-coupled PCM for polarization and spatial information recovery. The (polarization and modal-scrambling) multimode fiber is assumed to be linear with negligible loss.

$$\boldsymbol{E}^{(1)} = \sum_{n=1}^{N} \left(a_{xn}^{(1)}\boldsymbol{e}_{xn} + a_{yn}^{(1)}\boldsymbol{e}_{yn}\right) = \begin{pmatrix} a_{x1}^{(1)} \\ \vdots \\ a_{xN}^{(1)} \\ a_{y1}^{(1)} \\ \vdots \\ a_{yN}^{(1)} \end{pmatrix} \equiv \begin{pmatrix} A_x^{(1)} \\ A_y^{(1)} \end{pmatrix} \tag{1}$$

where N is the total number of the fiber-guided modes in one polarization, $\boldsymbol{e}_{xn}$ is the nth transverse fiber-guided mode which is predominantly x-polarized, $\boldsymbol{e}_{yn}$ is the nth y-polarized mode, and $A_x^{(1)}$ and $A_y^{(1)}$ are column vectors of rank N whose elements are the complex amplitudes $a_{xn}^{(1)}$ and $a_{yn}^{(1)}$, respectively. Note that the coupling into the other possible fiber modes (e.g., leaky and radiation modes) is neglected for simplicity of the analysis. The propagation left to right through the fiber, including the intermodal coupling, can be represented by the following matrix form:

$$\boldsymbol{E}^{(2)} = M\boldsymbol{E}^{(1)} \tag{2}$$

where M is the scattering matrix of the fiber in the forward direction and is given by

$$M = \begin{pmatrix} M_{xx} & M_{xy} \\ M_{yx} & M_{yy} \end{pmatrix} \tag{3}$$

in which $M_{ij}(i, j = x, y)$ are $N \times N$ submatrices. The field $\boldsymbol{E}^{(2)}$ is then passed through the polarizer and phase conjugated by the PCM, so the field $\boldsymbol{E}^{(3)}$ can be written as

$$\boldsymbol{E}^{(3)} = rCM^*(\boldsymbol{E}^{(1)})^* \tag{4}$$

where r is the PCM amplitude reflectivity and the matrix C, representing the removal of the y polarization by the polarizer, is given by

$$C = \begin{pmatrix} I & 0 \\ 0 & 0 \end{pmatrix}, \tag{5}$$

where I is an $N \times N$ unit matrix. A more general form of the matrix C will be considered in Section IV where nonreciprocal and/or amplitude distortions prior to the PCM are taken into account.

The output field $\boldsymbol{E}^{(4)}$ is expressed as

$$\boldsymbol{E}^{(4)} = rM'CM^*(\boldsymbol{E}^{(1)})^* \tag{6}$$

where M' is the scattering matrix for the reverse propagation in the fiber. Note that a mode-independent (scalar) reflectivity r of the PCM is assumed in (6). If a mode-dependent reflectivity is taken into account, r should be replaced by a $2N \times 2N$ diagonal matrix. This effect will be considered later in this section.

In what follows the properties of the scattering matrices are examined and the fields $\boldsymbol{E}^{(2)}$ and $\boldsymbol{E}^{(4)}$ are expressed in terms of the scattering matrix elements. First, because of the conservation of the energy in a lossless linear fiber the following unitarity condition is required:

$$M^\dagger M = \begin{pmatrix} I & 0 \\ 0 & I \end{pmatrix} \tag{7}$$

where † denotes the Hermite transpose operation.

Second, consider the ideal case of scalar phase conjugation by the PCM with the polarizer removed (i.e., the case where the field $\boldsymbol{E}^{(2)}$ is completely phase conjugated). In this case, viewing the fiber as some arbitrary lossless linear dielectric medium, the time-reversal symmetry of any fields applies and we must recover the original field $\boldsymbol{E}^{(4)} = r(\boldsymbol{E}^{(1)})^*$. This happens when

$$M'M^* = \begin{pmatrix} I & 0 \\ 0 & I \end{pmatrix}. \tag{8}$$

From (7) and (8) it is found that

$$M' = M^t \tag{9}$$

where t denotes the transpose operation. Here we note that the elements of the scattering matrices are interrelated by the constraint stated by (7) and (9). These constraints can be translated into the sum rules [26] which are used to find the results shown further on.

B. Spatial and Polarization Properties of the Field $\boldsymbol{E}^{(2)}$

With the relation $\boldsymbol{E}^{(2)} = M\boldsymbol{E}^{(1)}$ the correlations between the $2N$ modes of the field $\boldsymbol{E}^{(2)}$ can be expressed by means of the following $2N \times 2N$ Hermitian coherency matrix:

$$L^{(2)} \equiv \langle \boldsymbol{E}^{(2)}\boldsymbol{E}^{(2)\dagger} \rangle = M\langle \boldsymbol{E}^{(1)}\boldsymbol{E}^{(1)\dagger} \rangle M^\dagger = \begin{pmatrix} L_{xx}^{(2)} & L_{xy}^{(2)} \\ L_{xy}^{(2)\dagger} & L_{yy}^{(2)} \end{pmatrix} \tag{10}$$

where $\langle \cdots \rangle$ denotes the time average and $L_{ij}^{(2)}$ $(i, j = x, y)$ are $N \times N$ matrices. We note that the effect of possible decrease of the temporal coherence of the light source at the output, which is due to the modal dispersion in the fiber [34], is not taken into account in the present

analysis. This implies the assumption of a coherence time of the light source that is long enough to neglect the above effect.

The following "modified" 2 × 2 coherency matrix is now introduced:

$$J^{(2)} \equiv \begin{pmatrix} J_{xx}^{(2)} & J_{xy}^{(2)} \\ J_{xy}^{(2)*} & J_{yy}^{(2)} \end{pmatrix}. \tag{11}$$

Since the partition of the total power among the x and y polarization components in the field $\boldsymbol{E}^{(2)}$ is of interest, each element $J_{ij}^{(2)}$ $(i, j = x, y)$ in (11) is defined as

$$\begin{aligned} J_{ij}^{(2)} &= \sum_{k=1}^{N} \sum_{l=1}^{N} \iint_{\sigma} (L_{ij}^{(2)})_{kl} e_{ik} e_{jl}^{*} \, dx \, dy \\ &= (\text{const}) \times \sum_{k=1}^{N} (L_{ij}^{(2)})_{kk} \\ &= (\text{const}) \times \text{Tr}\,(L_{ij}^{(2)}). \end{aligned} \tag{12}$$

In (12) Tr denotes a trace of a matrix and the orthogonality of the fiber modes [35] is used, i.e., $\iint_{\sigma} e_{im} e_{jn}^{*} \, dx \, dy = (\text{const}) \times \delta_{mn}$ $(i, j = x, y; m, n = 1, \cdots, N)$, where σ denotes the whole fiber cross section and a circular fiber is assumed. It is seen from (12) that the off-diagonal elements of $L_{xx}^{(2)}$, $L_{xy}^{(2)}$, and $L_{yy}^{(2)}$ do not contribute to $J^{(2)}$ upon the detection of the field $\boldsymbol{E}^{(2)}$ over σ. We note that, unlike the usual definition of the coherency matrix [36], the elements of $J^{(2)}$ have the dimensionality of power (hereafter, however, we omit the constant in (12) for brevity).

For the sake of simplicity the x-polarized input is considered here. Then the diagonal elements of the submatrices $L_{ij}^{(2)}$ in (10) can be written as follows:

$$\begin{aligned} (L_{xx}^{(2)})_{ii} &= (M_{xx})_{ik} (M_{xx})_{ik'}^{*} (L_{xx}^{(1)})_{kk'} \\ &= |(M_{xx})_{ik}|^2 (L_{xx}^{(1)})_{kk} + (M_{xx})_{ik} (M_{xx})_{ik'}^{*} (L_{xx}^{(1)})_{\substack{kk' \\ (k \neq k')}} \end{aligned} \tag{13a}$$

$$(L_{yy}^{(2)})_{ii} = |(M_{yx})_{ik}|^2 (L_{xx}^{(1)})_{kk} + (M_{yx})_{ik} (M_{yx})_{ik'}^{*} (L_{xx}^{(1)})_{\substack{kk' \\ (k \neq k')}} \tag{13b}$$

$$(L_{xy}^{(2)})_{ii} = (M_{xx})_{ik} (M_{yx})_{ik'}^{*} (L_{xx}^{(1)})_{kk'} \tag{13c}$$

where $(L_{xx}^{(1)})_{ij} \equiv (\langle \boldsymbol{E}^{(1)} \boldsymbol{E}^{(1)\dagger} \rangle_{xx})_{ij}$ denotes the correlations between the N modes of the x-polarized input field, and henceforth summation over repeated indexes [but not over i in (13)] is understood. At this point because of the strong intermodal coupling in the fiber the amplitudes of the matrix elements M_{ij}, i.e., coupling strength between modes, are assumed to be essentially the same (or symmetrically and widely distributed with respect to the diagonal elements M_{ii}), while their relative phases are distributed essentially uniformly over the $-\pi \sim +\pi$ interval (henceforth we refer this to *the random coupling approximation;* see Appendix A). We see from (13) that the input power initially coupled into any one fiber-guided mode is redistributed during propagation among all the other fiber-guided modes including those of the orthogonal y polarization. Consequently the out-coupled different spatial modes possessing random phases interfere with one another at any point, resulting in the speckled spatial structures in the free space.

The polarization state of the field $\boldsymbol{E}^{(2)}$ can be obtained using $J^{(2)}$. The following parameters are introduced:

$$a_{kk'} \equiv (M_{xx})_{ik} (M_{xx})_{ik'}^{*} \tag{14a}$$

$$b_{kk'} \equiv (M_{xx})_{ik} (M_{yx})_{ik'}^{*} \tag{14b}$$

$$d \equiv \sum_{k=1}^{N} (L_{xx}^{(1)})_{kk} \tag{15}$$

$$q \equiv \frac{2a_{kk'} (L_{xx}^{(1)})_{\substack{kk' \\ (k \neq k')}}}{d} \tag{16a}$$

and

$$u \equiv \frac{2b_{kk'} (L_{xx}^{(1)})_{kk'}}{d}. \tag{16b}$$

By substituting these parameters into (11)–(13) together with the sum rules from (7) and (9), it is found that

$$J_{xx}^{(2)} = a_{kk} (L_{xx}^{(1)})_{kk} + \tfrac{1}{2} q d \tag{17a}$$

$$J_{yy}^{(2)} = (1 - \tfrac{1}{2} q)\, d - a_{kk} (L_{xx}^{(1)})_{kk} \tag{17b}$$

$$J_{xy}^{(2)} = \tfrac{1}{2} u d. \tag{17c}$$

Here we note that the terms $a_{kk'(k \neq k')}$ and $b_{kk'}$ in (17) are much smaller than a_{kk} due to the modal averaging (see Appendix A), and that d is the total input power to the fiber. The Stokes parameters (s_0, s_1, s_2, s_3) and the degree of polarization $(P^{(2)})$ of the field $\boldsymbol{E}^{(2)}$ [36] are then given by

$$s_0 \equiv J_{xx}^{(2)} + J_{yy}^{(2)} = d \tag{18a}$$

$$s_1 \equiv J_{xx}^{(2)} - J_{yy}^{(2)} = 2a_{kk} (L_{xx}^{(1)})_{kk} - (1 - q)\, d \tag{18b}$$

$$s_2 \equiv J_{xy}^{(2)} + J_{yx}^{(2)} = [\text{Re}\,(u)]\, d \tag{18c}$$

$$s_3 \equiv i(J_{yx}^{(2)} - J_{xy}^{(2)}) = [\text{Im}\,(u)]\, d \tag{18d}$$

and

$$P^{(2)} = \frac{\sqrt{s_1^2 + s_2^2 + s_3^2}}{s_0}. \tag{19}$$

By using the random coupling approximation so that $a_{kk} \simeq 0.5$ for any k, $P^{(2)}$ is reduced to

$$P^{(2)} \simeq \sqrt{q^2 + |u|^2} \tag{20}$$

and the power emitted from the fiber at each polarization is given by

$$J_{xx}^{(2)} = \tfrac{1}{2}(1 + q)\, d \tag{21a}$$

and

$$J_{yy}^{(2)} = \tfrac{1}{2}(1 - q)\, d. \tag{21b}$$

We see that the residual polarization of the field $\boldsymbol{E}^{(2)}$ is due to the parameters q and u, and is in general much smaller than unity in the strong intermodal coupling regime. For the complete modal scrambling (i.e., q, $u = 0$) the output power is equally divided between both orthogonal polarizations, i.e., $J_{xx}^{(2)} = J_{yy}^{(2)} = d/2$, so that the field $\boldsymbol{E}^{(2)}$ is completely depolarized, i.e., $P^{(2)} = 0$. As will be seen from the experimental results in the next section, the field $\boldsymbol{E}^{(2)}$ exhibits spatial distortions and nearly-complete depolarization due to the strong intermodal coupling in the fiber, thus verifying the random coupling approximation and the modal averaging assumption. However the parameters q and u will play a role in the fidelity of the reconstruction of the original information, as discussed in the next subsection.

C. Spatial and Polarization Properties of the Field $\boldsymbol{E}^{(4)}$

In this subsection it will be shown that the spatially distorted and depolarized field $\boldsymbol{E}^{(2)}$ can be corrected, under certain conditions, even when only one polarization component of the field $\boldsymbol{E}^{(2)}$ is phase conjugated.

First, rewrite (6) as

$$\boldsymbol{E}^{(4)} = rS(\boldsymbol{E}^{(1)})^* \tag{22}$$

where the scattering matrix S in the round-trip propagation is given by $S = M'CM^*$. Here the random coupling approximation is again used so that $\Sigma_{i=1}^{N} |(M_{xx})_{ik}|^2$, $\Sigma_{i=1}^{N} |(M_{xy})_{ik}|^2 \simeq 0.5$. Then $S = S_1 + S_2$, where

$$S_1 = \tfrac{1}{2}\begin{pmatrix} I & 0 \\ 0 & I \end{pmatrix} \tag{23a}$$

and

$$S_2 = \begin{pmatrix} D & Q \\ Q^\dagger & D' \end{pmatrix} \tag{23b}$$

in which D, D', and Q are $N \times N$ submatrices given by

$$D_{ij} = \begin{cases} 0, & (i = j) \\ (M_{xx})_{ki}(M_{xx})_{kj}^*, & (i \neq j) \end{cases} \tag{24a}$$

$$D'_{ij} = \begin{cases} 0, & (i = j) \\ -(M_{yy})_{ki}(M_{yy})_{kj}^*, & (i \neq j) \end{cases} \tag{24b}$$

$$Q_{ij} = (M_{xx})_{ki}(M_{xy})_{kj}^*. \tag{24c}$$

The field $\boldsymbol{E}^{(4)}$ given by (22) becomes

$$\boldsymbol{E}^{(4)} = \tfrac{1}{2}r(\boldsymbol{E}^{(1)})^* + \boldsymbol{V} \tag{25}$$

where $\boldsymbol{V} = rS_2(\boldsymbol{E}^{(1)})^*$. We note that the decomposition of S given in (22) leads to the first term in (25), which corresponds to *a true phase-conjugate replica* of $\boldsymbol{E}^{(1)}$, and the second term in (25), which corresponds to *noise* possessing random phases.

Fig. 2 shows a diagrammatic explanation of the formation of the field $\boldsymbol{E}^{(4)}$. The x-polarized ith mode excited initially at the input plane of the fiber is coupled into all the fiber-guided modes at the output in the forward direction. After the elimination of the y-polarized component and phase conjugation of the x-polarized component each mode at the output plane is, again, coupled into all of the fiber-guided modes at the input plane in the backward direction. In Fig. 2(a) the (time-reversed) paths in the backward direction are exactly the same as those in the forward direction, resulting in a constructive coherent superposition of the scattered fields at each mode at the input plane. This constructive interference is expressed by the scattering matrix S_1, and the resulting true phase-conjugate field, corresponding to the term $r(\boldsymbol{E}^{(1)})^*/2$ in (25), has almost one-half of the total reflected power. On the other hand, in Fig. 2(b) the remainder of the paths in the backward direction are random and different from those in the forward direction. This random interference at each mode at the input plane is expressed by the scattering matrix S_2, and the resulting field forms the noise $\boldsymbol{V}$ given in (25). The total power of this noise is nearly the same as that of the true phase-conjugate field, but, as we will see later, it is distributed essentially uniformly among all of the fiber-guided modes independently of the input-beam numerical aperture (NA). Therefore the noise power per mode can be much smaller than that of the true phase-conjugate field, provided that the input field initially excites only a small fraction, say f, of the fiber-guided modes (i.e., that a small input-beam NA is used) and that the detection is made within such a small input NA. In this case we can, to the order of f, neglect such noise contributions $\boldsymbol{V}$ in (25), and the detected part of the field $\boldsymbol{E}^{(4)}$ can be the true phase-conjugate replica of the input field $\boldsymbol{E}^{(1)}$ [21]–[23], [25], [26]. (Also see Appendix B for the qualitative proof of (25).) It is interesting to note that the above round-trip (time-reversed) scattering process is reminiscent of localization and coherent backscattering of photons in disordered media [37], which has recently attracted a great deal of attention mainly in connection with analogous phenomena on Anderson localization of electrons [38].

The correlations between the $2N$ modes of the field $\boldsymbol{E}^{(4)}$ can also be expressed by means of the following $2N \times 2N$ Hermitian coherency matrix:

$$\begin{aligned} L^{(4)} &\equiv \langle \boldsymbol{E}^{(4)}\boldsymbol{E}^{(4)\dagger} \rangle \\ &= |r|^2 S L^{(1)*} S^\dagger \\ &= |r|^2 [\tfrac{1}{4}L^{(1)*} + S_2 L^{(1)*} S_2^\dagger + \tfrac{1}{2}(S_2 L^{(1)*} + L^{(1)*} S_2^\dagger)]. \end{aligned} \tag{26}$$

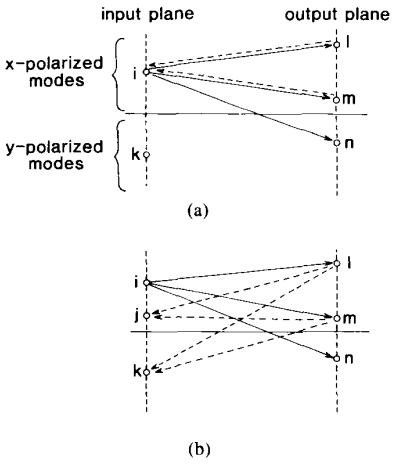

Fig. 2. Diagrammatic description of the formation of the field $E^{(4)}$: (a) deterministic phase-conjugate paths which result in true phase conjugation of the input field $E^{(1)}$; (b) randomly scattered phase-conjugate paths which result in the noise.

On the right-hand side of the above equation the first term corresponds to a time-reversed polarization state of the input field $E^{(1)}$, while the rest of the terms correspond to the noise. It is again sufficient to consider the case of the x-polarized incidence. In this case the noise terms in (26) can be expressed in terms of the submatrices D and Q given in (23b). Then it can be shown [26] that the noise consists of the following two contributions: 1) "the depolarized noise" which comes from the second term of the right-hand side of (26). The ratio of this noise power to the true phase-conjugate beam power per mode is of the order of M_0/N (M_0 is the number of the fiber-guided modes that are excited initially), independently of the mode number. This noise contribution has also been reported by Wabnitz [25]; 2) "the polarized noise" which comes from the third term in (26) and its ratio to the true phase-conjugate beam power is of the order of $|q|$. Although this noise is x-polarized and resides within the mode number M_0, its spatial structure is distorted due to the random phases. These two noise contributions can be, however, negligibly small when $M_0/N \ll 1$ and $|q| \ll 1$, that is, when a small input NA is used and the field $E^{(2)}$ is nearly-completely depolarized (i.e., in the strong intermodal coupling regime).

The polarization recovery of the field $E^{(1)}$ can now be evaluated quantitatively. Suppose that the whole power of the field $E^{(4)}$ is detected. Then the polarization state of the field $E^{(4)}$ is expressed by means of the following 2×2 modified coherency matrix of the field $E^{(4)}$:

$$J^{(4)} \equiv \begin{pmatrix} J_{xx}^{(4)} & J_{xy}^{(4)} \\ J_{xy}^{(4)*} & J_{yy}^{(4)} \end{pmatrix} = \tfrac{1}{4}|r|^2 J^{(1)*} + J_{\text{noise}}^{(4)} \tag{27}$$

where

$$J^{(1)} = \begin{pmatrix} d & 0 \\ 0 & 0 \end{pmatrix} \tag{28a}$$

and

$$J_{\text{noise}}^{(4)} = \begin{pmatrix} \text{Tr}\,(L_{xx}^{(4)}) - \tfrac{1}{4}|r|^2 d & \text{Tr}\,(L_{xy}^{(4)}) \\ \text{Tr}\,(L_{xy}^{(4)\dagger}) & \text{Tr}\,(L_{yy}^{(4)}) \end{pmatrix} \tag{28b}$$

in which the total power of the x-polarized input d is given by (15) and $L^{(4)}$ by (26). After some lengthy calculations using (26)–(28) together with the sum rules from (7) and (9), the total noise power P_N is given by

$$P_N \equiv \text{Tr}\,(J_{\text{noise}}^{(4)}) = \tfrac{1}{4}|r|^2 d(1 + 2q) \tag{29}$$

where $q(|q| \ll 1)$ is given by (16a). It is seen from (27)–(29) that almost one-half of the reflected power is from the noise and the rest is from the true phase-conjugate beam. From the explicit expression of (26) it can be shown [26] that it is appropriate to assume that the depolarized noise power in the field $E^{(4)}$ is distributed among all the fiber-guided modes and the total noise power of the x polarization is nearly the same as that of the y polarization. Consequently the 2×2 coherency matrix of the noise can be written as

$$J_{\text{noise}}^{(4)} \simeq \lambda \begin{pmatrix} 1 + 4q & 2v \\ 2v^* & 1 \end{pmatrix} \tag{30}$$

where $\lambda \equiv |r|^2 d/8$, $v \equiv 2Q_{li}(L_{xx}^{(1)})_{li}/d(|v| \ll 1)$, and the terms which are of smaller orders of magnitude due to the complete phase mismatching are neglected. From (27)–(30) the degree of polarization of the total integrated intensity of the field $E^{(4)}$ is given by

$$P^{(4)} \simeq \frac{1 + 2q}{2(1 + q)} \tag{31a}$$

and the reflectivity R, defined as a ratio of the x-polarized reflected power to the input beam power for the x-polarized input, is given by

$$R \equiv \frac{J_{xx}^{(4)}}{d} = \frac{1}{8}|r|^2(3 + 4q) \tag{31b}$$

where the definition of the degree of polarization is given by (19) and the second-order terms in q and v are neglected. It is seen from (31) that $P^{(4)}$ and R depend on the residual polarization of the field $E^{(2)}$, i.e., nonzero values of q. Furthermore the degree of polarization recovery p [19], which is defined as $p \equiv (J_{xx}^{(4)} - J_{yy}^{(4)})/(J_{xx}^{(4)} + J_{yy}^{(4)})$, i.e., the recovery of the linearly x-polarized component, is found to be equal to $P^{(4)}$ to the first order in q and v. Likewise if a linearly y-polarized light is used as an input, the same results with $q \equiv 2D_{il}'(L_{yy}^{(1)})_{il}^*/d$ can be obtained. Finally if the field $E^{(2)}$ is completely depolarized (i.e., $q = v = 0$), it is found that

$$J_{\text{noise}}^{(4)} \simeq \begin{pmatrix} \lambda & 0 \\ 0 & \lambda \end{pmatrix} \tag{32}$$

so that the noise field in the field $E^{(4)}$ is also completely depolarized and one-half of the reflected power is equally distributed among all the fiber modes of both polarizations. In this case the degree of polarization $P^{(4)}$ and the reflectivity R of the total integrated intensity of the field $E^{(4)}$ becomes 0.5 and $3|r|^2/8$, respectively. This asymptotic result was observed experimentally and explained theoretically by two groups [22], [23].

In practice, however, the input field $E^{(1)}$ excites only a fraction of all the fiber-guided modes (i.e., the input-beam NA is smaller than the fiber's NA), as was the case in the first experimental observation [19]. In this case the detection is usually made only within the same (input-beam) NA. Therefore the total noise power within the detection area is smaller than the total noise power discussed above. To see the effect of the input-beam NA on the degree of polarization $P^{(4)}$, the following modal partition functions for the true phase-conjugate field and the noise field are introduced, respectively [22], [26]:

$$\Theta_i \equiv \frac{\text{true phase-conjugate power in the } i\text{th mode}}{2\lambda} \tag{33a}$$

$$\Lambda_i \equiv \frac{\text{polarized noise power in the } i\text{th mode}}{4q\lambda} \tag{33b}$$

$$\Delta_i \equiv \frac{\text{depolarized noise power in the } i\text{th mode of each polarization}}{\lambda}. \tag{33c}$$

By using these partition functions and the maximum mode number M upon the detection and then by diagonalizing $J^{(4)}$, the polarized power P_{pol} and the depolarized noise power P_M can be expressed as

$$P_{\text{pol}} = 2\lambda\left(\sum_{i=1}^{M}\Theta_i + 2q\sum_{i=1}^{M}\Lambda_i\right) \tag{34a}$$

and

$$P_M = 2\lambda\sum_{i=1}^{M}\Delta_i \tag{34b}$$

where the contributions of the off-diagonal elements in $L^{(4)}$ and of the second order terms in q and v are neglected. Then the degree of polarization $P^{(4)}$ and the reflectivity R upon the detection are given by

$$P^{(4)} \equiv \frac{P_{\text{pol}}}{P_{\text{pol}} + P_M} = \frac{1 + 2q\beta_1}{1 + 2q\beta_1 + \beta_2} \tag{35a}$$

and

$$R = \frac{1}{8}|r|^2\sum_{i=1}^{M}\Theta_i(2 + 4q\beta_1 + \beta_2) \tag{35b}$$

where

$$\beta_1 \equiv \frac{\sum_{i=1}^{M}\Lambda_i}{\sum_{i=1}^{M}\Theta_i} \tag{36a}$$

and

$$\beta_2 \equiv \frac{\sum_{i=1}^{M}\Delta_i}{\sum_{i=1}^{M}\Theta_i}. \tag{36b}$$

It is seen that $P^{(4)}$ is again equal to the degree of polarization recovery p, and $P^{(4)}$ and R are reduced to (31) as $M \to N$.

So far r has been treated as a scalar value, i.e., r is independent of the spatial structure of the field $E_x^{(2)}$. Since the field $E^{(2)}$ emitted from the fiber has a large field-of-view, the fidelity of phase-conjugate field $E^{(3)}$ reflected by the PCM may be degraded due to the spatial frequency dependence of a phase-conjugate reflectivity of the PCM. To take this possible degradation into account, a scalar quantity r should be replaced by a $2N \times 2N$ diagonal matrix. Then by using the same argument as before and introducing "the efficiency" η $(0 < \eta \leq 1)$ that denotes a fractional power of the true phase-conjugate field $E_x^{(2)*}$ in the total power of the field $E^{(3)}$ reflected by the PCM, the following general formulas for $P^{(4)}$ and R can be obtained [26]:

$$P^{(4)} = \frac{1 + 2q\beta_1}{1 + 2q\beta_1 + [1 + 2(\epsilon - 1)(1 + q)]\beta_2} \tag{37a}$$

and

$$R = \frac{1}{8\epsilon}|r|^2\sum_{i=1}^{M}\Theta_i\{2 + 4q\beta_1 + [1 + 2(\epsilon - 1)(1 + q)]\beta_2\} \tag{37b}$$

where $\epsilon \equiv \eta^{-1}$, and it is assumed that the field $E^{(3)}$ contains the possible "wrong" phase-conjugate field $E_w^{(3)}$ so that the field $E_w^{(3)}$ causes the additional depolarized field $E_w^{(4)}$ which has the same partition function as Δ_i.

Consider now two specific forms of the modal partition functions. A uniform distribution of the depolarized noise field gives

$$\sum_{i=1}^{M}\Delta_i = \frac{M}{N}. \tag{38}$$

In the case of a Gaussian distribution the discrete modal intensity is replaced by a continuous one for a large N, that is,

$$I_d = I_0 \exp\left(-\frac{8r^2}{\psi^2}\right) \tag{39}$$

where I_d is the "average" depolarized noise intensity in each polarization in the detection plane (which is usually a far-field plane of the fiber end), ψ is an effective diameter of the depolarized noise intensity distribution in the detection plane, and $I_0 = |r|^2\, d/\psi^2\pi$ so that $\iint_{-\infty}^{\infty} I_d\, dx\, dy = |r|^2\, d/8$. It is then found that

$$\sum_{i=1}^{M} \Delta_i \simeq 1 - \exp\left[-2(\phi/\phi_0)^2/(\psi/\phi_0)^2\right] \tag{40}$$

where

$\phi_0 \equiv$ the input-beam diameter corresponding to N

and

$\phi \equiv$ the input-beam diameter corresponding to M

so that the parameter $(\phi/\phi_0)^2$ is equal to M/N and to (input-beam NA/fiber's NA)^2 [39].

Fig. 3 shows the theoretical curves of (a) R/R_0 ($R_0 \equiv |r|^2\, d(1 + 2q)/4\epsilon$) and (b) $P^{(4)}$ as a function of $(\phi/\phi_0)^2$ (i.e., input-beam NA) for a uniform and a Gaussian ($\psi/\phi_0 = 0.5$) distribution, where, according to the experimental situation, $M = M_0$ is used so that $\Sigma_{i=1}^{M} \Theta_i = 1$ and $\beta_1 = 1$, i.e., the detection aperture is the same as the input-beam NA. Three values of q's ($q = 0, \pm 0.035$) are used to see the effect of the residual polarization of the field $E^{(2)}$. These values correspond to $P^{(2)} = 0, 0.05$, respectively, when $|q| \simeq |u|$ is assumed [see (20)]. Here $\eta = 1$ ($\epsilon = 1$) is used, i.e., the PCM faithfully phase conjugates the field $E_x^{(2)}$. It is seen that $P^{(4)}$ decreases as $(\phi/\phi_0)^2$ increases. Note, however, that when the input-beam NA is much smaller than the fiber's NA (i.e., $(\phi/\phi_0)^2 \ll 1$), then $P^{(4)}$ is close to unity, i.e., *almost complete polarization recovery* is possible. This is because the noise power is distributed among all the fiber-guided modes so that for a small input-beam NA the noise power contained within such a small fraction of all the fiber-guided modes can be negligible compared to that of the true phase-conjugate beam. We see that the behavior of $P^{(4)}$ and R is sensitive to the forms of the noise distribution and the values of q's. When q is negative, the values of R and $P^{(4)}$ are higher than those for $q \geq 0$. This is because the residual x-polarized power is increased independently of q and $R_0|_{q>0} > R_0|_{q<0}$. We also see that as $(\phi/\phi_0)^2$ approaches unity, R/R_0 increases up to 1.5 while $P^{(4)}$ decreases down to 0.5 for $q = 0$. As mentioned above, this asymptotic behavior was previously pointed out in [22] and [23].

D. SNR of the Reconstructed Spatial Information

In this subsection the SNR of the reconstructed spatial information in the present phase-conjugation process is considered. As mentioned at the beginning of this section, the statistical treatment is employed here. Goodman [40] has analyzed the SNR which is defined as the ratio of the deterministic image intensity I_s to the rms value of σ_I of the total image intensity at the same point, in a reconstructed image by a hologram. In the present case, we note the following features of the field $E^{(4)}$ (for the sake of simplicity the case of $q = 0$ and $\eta = 1$ is considered in the following calculation).

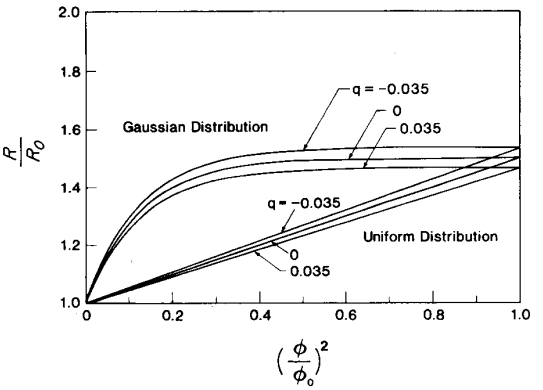

(a)

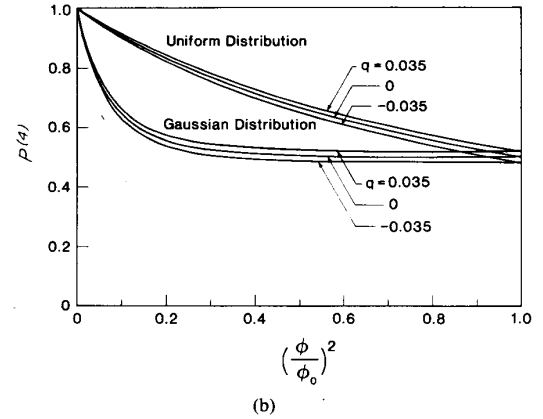

(b)

Fig. 3. Theoretical curves as a function of $(\phi/\phi_0)^2$ for a uniform and a Gaussian noise distribution ($\psi/\phi_0 = 0.5$). The values $q = 0, \pm 0.035$ and $\eta = 1$ are used. (a) The normalized reflectivity R/R_0. (b) The degree of polarization $P^{(4)}$.

1) The true phase-conjugate field acts as a coherent background intensity I_s in the x-polarized intensity.

2) The speckle noise field is completely depolarized so that there is no correlation between two orthogonal x- and y-polarized components, and that such speckle intensities in both polarizations are equal at one point in the detection plane.

3) Each polarized component of the speckle noise field is fully developed and therefore its intensity statistics obeys a negative exponential distribution.

It is then found [26] that the total characteristic function [41] for the field $E^{(4)}$ is given by

$$\Phi_I(iv) = \frac{1}{(1 - iv\bar{I}_{\text{noise}})^2} \cdot \exp\left[-\frac{I_s}{\bar{I}_{\text{noise}}} + \frac{I_s}{\bar{I}_{\text{noise}}(1 - iv\bar{I}_{\text{noise}})}\right], \tag{41}$$

where $\bar{I}_{noise}$ is the ensemble averaged speckle noise intensity of one polarization at one point in the detection plane. The rms noise intensity is then given by

$$\sigma_I = \left[2\bar{I}_{noise}(\bar{I}_{noise} + I_s)\right]^{1/2}. \tag{42}$$

Consequently the SNR can be written as

$$(\mathrm{SNR})_{xy} \equiv \frac{I_s}{\sigma_I} = \gamma\sqrt{\frac{2}{1+2\gamma}} \tag{43}$$

where $\gamma = I_s/2\bar{I}_{noise}$ is the "beam ratio" parameter [41]. If an analyzer (set to the x polarization direction) is used to measure only the x-polarized component of the field $E^{(4)}$, then the SNR can be found straightforwardly to be

$$(\mathrm{SNR})_x = \frac{2\gamma}{\sqrt{1+4\gamma}}. \tag{44}$$

To illustrate the dependence of these SNR's on the input-beam NA, we identify $I_s = |r|^2\, d/(\pi\phi^2)$ [i.e., the input is assumed to be a two-dimensionally uniform beam with the diameter ϕ so that the total power of the true phase-conjugate beam is $|r|^2\, d/4$. See also (27)] and $\bar{I}_{noise}$ is given by $|r|^2\, d/(2\pi\phi_0^2)$ for a uniform distribution and by I_d [see (39)] for a Gaussian distribution. Then the beam ratio parameter γ at the center of the signal beam is given by

$$\gamma = \begin{cases} \dfrac{1}{\left(\dfrac{\phi}{\phi_0}\right)^2}, & \text{for a uniform distribution} \\ \dfrac{1}{2}\dfrac{\left(\dfrac{\psi}{\phi_0}\right)^2}{\left(\dfrac{\phi}{\phi_0}\right)^2}, & \text{for a Gaussian distribution.} \end{cases}$$

Fig. 4 shows the dependence of the two SNR's, as given by (43) and (44), on $(\phi/\phi_0)^2$ at the center of the true phase-conjugate beam for a uniform and a Gaussian $(\psi/\phi_0 = 0.5)$ distribution. It is seen that for the Gaussian distribution the two SNR's decrease rapidly when $(\phi/\phi_0)^2$ exceeds about 0.01, i.e., the input-beam NA exceeds about 10 percent of the fiber NA, while for the uniform distribution the changes of the SNR's are slower. This is because given a deterministically constant value of the phase-conjugate reflective power (i.e., $|r|^2 d/4$), the intensity I_s at the center of the phase-conjugate beam decreases as the input-beam NA increases, while the noise intensity I_{noise} is almost constant independently of the input-beam NA, resulting in decrease of γ. It is also seen that the $(\mathrm{SNR})_{xy}$ and the $(\mathrm{SNR})_x$ are almost the same over an entire range of the input-beam NA's. This indicates that although an analyzer is inserted in order to eliminate unwanted speckle noise of the orthogonal polarization, the improvement of the SNR is very small [42]. Finally it should be noted that the qualitative dependence of the SNR on the input-beam NA is the same as that of the degree of polarization shown in Fig. 3(b), although the SNR in a linear scale seems to be more sensitive to the input-beam NA.

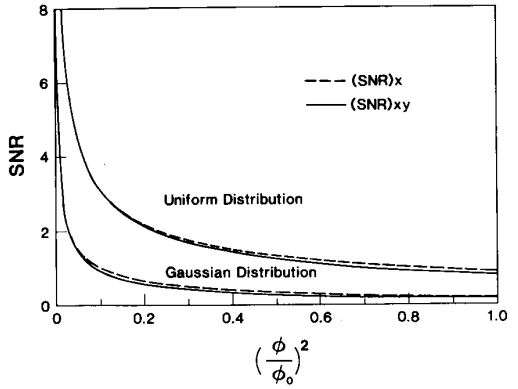

Fig. 4. Theoretical curves of the two SNR's, $(\mathrm{SNR})_{xy}$ and $(\mathrm{SNR})_x$ at the center of the signal beam, as a function of $(\phi/\phi_0)^2$ for a uniform and a Gaussian noise distribution $(\psi/\phi_0 = 0.5)$. The values $q = 0$ and $\eta = 1$ are used.

III. Experiments

In this section the experimental observation of polarization and spatial information recovery by modal dispersal and phase conjugation [19] is described. Then the experimental results of the fidelity of the phase conjugation process [22] are shown and compared with the theory described in the previous section.

A. Polarization and Spatial Information Recovery for Small NA Inputs

The experimental arrangement is shown in Fig. 5 [19]. The input-beam NA was about 0.01, which was much smaller than the fiber's NA. If $E^{(4)}$ is the true phase-conjugate replica of $E^{(1)}$ (including the polarization state), then the output light $E^{(5)}$ having retraversed the wave plate must return to the complex conjugate of the initial x-polarized state $E^{(0)}$. Thus the degree of polarization recovery $p = (P_1 - P_2)/(P_1 + P_2)$ defined in the previous section can be a measure of the polarization recovery, where P_1 and P_2 are, respectively, the power of the two orthogonal polarization components of $E^{(5)}$. In Fig. 5(b), the y-polarized, rather than the x-polarized, component of $E^{(2)}$ was used to generate the phase-conjugate field. Since the crystal reflects preferentially the x-polarized field, the polarization direction was rotated by 90° by the $\lambda/2$ plate prior to incidence of the crystal.

Fig. 6 shows the experimentally observed dependence of p as a function of the direction of polarization (φ) of the linearly polarized light entering the fiber. This direction was controlled by the angular position of the $\lambda/2$ plate. The quantity p is seen to be very nearly unity over the whole range, indicating a very good (better than 96 percent) restoration of the original linear polarization.

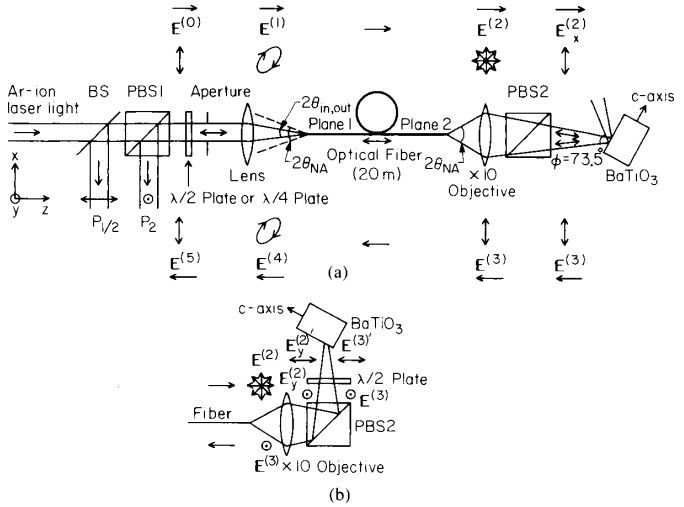

Fig. 5. Experimental arrangement for polarization and spatial information recovery. In (a), the x-polarized component $E_x^{(2)}$ in the depolarized light $E^{(2)}$ is used to generate the phase-conjugate beam. In (b), the y-polarized component $E_y^{(2)}$ is used.

Also plotted in Fig. 6 is the reflectivity R_1 of the phase conjugator defined by $R_1 = P_1/P_0$ (P_0 = input beam power at the crystal). When arbitrary elliptically-polarized light was used as the input $E^{(1)}$, p was also close to unity. Fig. 7 shows p and R_1 as a function of P_0 for the three different polarization states at the input: linearly polarized, circularly polarized, and elliptically polarized. The quantity p is seen to be also close to unity for the inputs of several polarization states, indicating the complete reversal of an arbitrary polarized input beam whose input-beam NA is much smaller than the fiber's NA: in this experiment $(\phi/\phi_0)^2 = 0.001$ [see the theoretical curves at this input-beam NA shown in Fig. 3(b)]. These results were obtained for both of the experimental arrangement of Fig. 5(a) and (b). The spatial recovery of the input $E^{(1)}$ (a uniform beam in the experiment) was also observed with high quality (see [19, Fig. 2]).

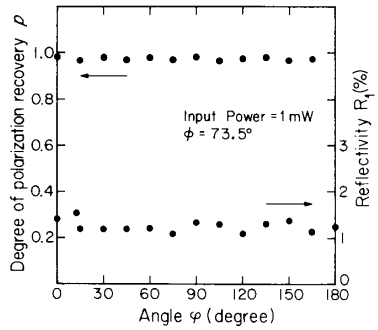

Fig. 6. Degree of polarization recovery p and reflectivity R of the fiber-coupled PCM are plotted as a function of the angle φ between the polarization direction of the input linearly polarized beam and the x axis.

B. Fidelity of Phase Conjugation

Several experiments were also performed in order to determine the fidelity of the phase-conjugation process as a function of the input-beam NA [22]. The experimental arrangement is shown in Fig. 8. The x-polarized input beam $E^{(1)}$ from the multilongitudinal-mode argon-ion laser beam (λ = 514.5 nm) was focused into the multimode (0.29 NA, 5 m long) graded-index fiber through a lens (L1). The input-beam diameter ϕ (and therefore the input-beam NA which we will also designate by ϕ) was controlled by an aperture (AP1). The phase-conjugate beam $E^{(4)}$ from the input end of the fiber is reflected by the nonpolarizing beam splitter (BS1). An aperture (AP2) with a diameter Φ was placed in front of the $\lambda/4$ plate to limit the detecting area for $E^{(4)}$.

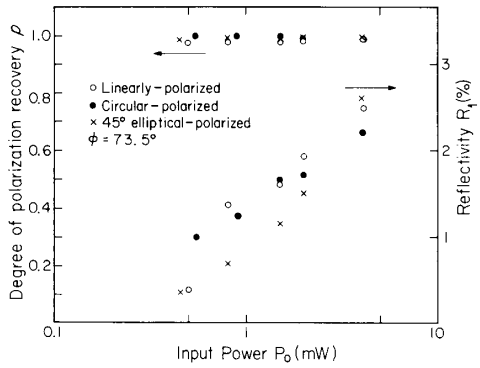

Fig. 7. Degree of polarization recovery p and reflectivity R_1 of the fiber-coupled PCM are plotted as a function of the input power P_0 for the three different input polarization states: linearly polarized (○), circularly polarized (●), and 45° elliptically polarized (×).

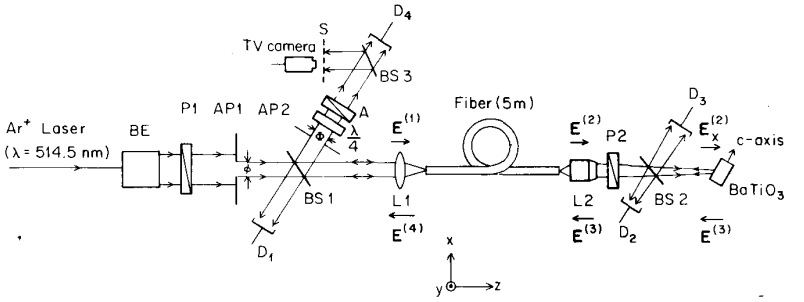

Fig. 8. Experimental arrangement. BE: beam expander; P1, P2: polarizers to guarantee the x-polarized input to the fiber and the crystal, respectively; D1, D2, D3: detectors for measuring the power of the beams $E^{(1)}$, $E_x^{(2)}$ and $E^{(3)}$, respectively.

The measured polarization states of the field $E^{(2)}$ for the different values of the input-beam NA's are shown in Table I [26]. It is seen that s_1, s_2, and s_3 are much smaller than s_0, so the degree of polarization is much smaller than unity, i.e., the beam $E^{(2)}$ is almost completely depolarized, independently of the input-beam NA. These data clarify the validity of the random coupling approximation and the modal averaging assumption (i.e., the assumption that due to random phases of M_{ij}'s the cross terms $a_{kk'(k \neq k')}$ and $b_{kk'}$ given by (14) and also q and u given by (16) are much smaller than unity).

Fig. 9 shows the experimental results of R ($\equiv |E_x^{(4)}/E^{(1)}|^2$) [Fig. 9(a)] and $P^{(4)}$ and p [Fig. 9(b)], as a function of $(\phi/\phi_0)^2$ for the linearly x-polarized input ($p, P^{(1)} > 0.99$). The theoretical plots of R and $P^{(4)}$ from (37) are also shown using the Gaussian distribution of the noise intensity ($\psi/\phi_0 = 0.5$), and $(q, \eta) = (0, 1)$, $(0.035, 1)$, $(0, 0.8)$ and $(0.035, 0.8)$ [26]. According to the data shown in Table I, a positive value of q ($= 0.035$) was used in the theoretical calculation. (Note that $s_1 > 0$ corresponds to $q > 0$. See (18b) with $a_{kk} \simeq 0.5$.) Since the experimental data of R included unwanted losses due to reflection and absorption by optical components, the proportionality factors in the theoretical curves of R were determined by the least squares fit with the experimental data. The diameter Φ of AP2 was set to be $\Phi = \phi$ for all ϕ's. All the data were obtained within uncertainties of ± 10 percent. It is shown that for very small ϕ (i.e., when the input-beam NA is very small compared to the fiber's NA), p is almost unity, i.e., true phase conjugation of the input beam $E^{(1)}$ is possible, whereas R is low. On the other hand, p decreases appreciably by an increase of ϕ, accompanied with the increase in R. It is also seen that $p \approx P^{(4)}$ for all ϕ's, indicating that the polarized part of the phase-conjugate beam is almost x-polarized and that the rest of the phase-conjugate beam is completely depolarized. Thus the power in the depolarized component of the reflected beam increases with the increase of ϕ, making the total R increase but p and $P^{(4)}$ decrease. Note that the theoretical curves are in good agreement with the experimental data when the Gaussian distribution of the noise intensity, the residual polarization of the field $E^{(2)}$, and the fidelity of the PCM are taken into account (i.e.,

TABLE I
EXPERIMENTAL DATA OF THE STOKES PARAMETERS AND THE DEGREE OF POLARIZATION OF THE FIELD $E^{(2)}$

Input-Beam NA	s_1/s_0	s_2/s_0	s_3/s_0	$P^{(2)}$
0.02	0.003	0.008	−0.016	0.018
0.11	0.033	0.023	−0.028	0.049
0.25	0.004	0.041	−0.021	0.046

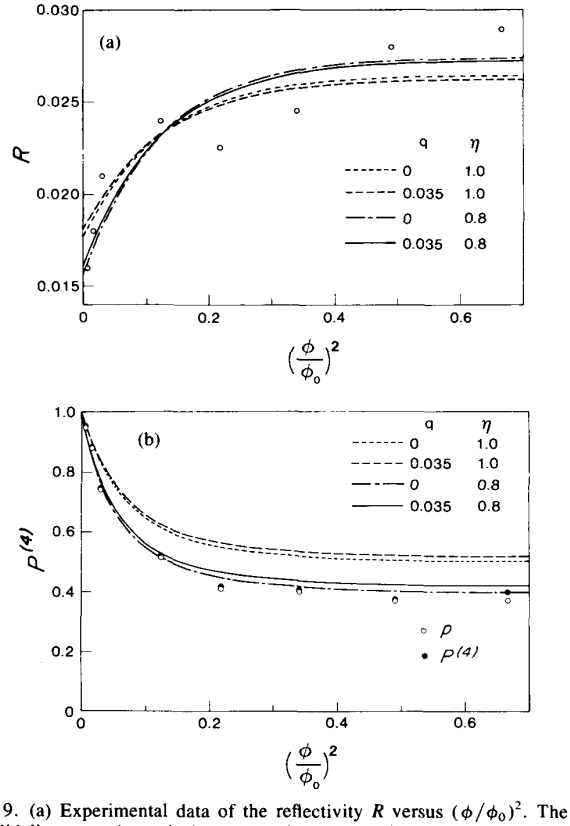

Fig. 9. (a) Experimental data of the reflectivity R versus $(\phi/\phi_0)^2$. The solid lines are theoretical curves using a Gaussian noise distribution ($\psi/\phi_0 = 0.5$) and $(q, \eta) = (0, 1)$, $(0, 0.8)$, $(0.035, 1)$, and $(0.035, 0.8)$. The proportional factor of R in the theoretical calculation is determined by the least squares fit with the experimental data shown here. (b) Experimental data of the degree of polarization recovery p(○) and the degree of polarization $P^{(4)}$(●). The solid lines are theoretical curves whose parameters are the same as those in (a).

(a) (b)

Fig. 10. Photographs of the x-polarized phase-conjugate images of the letter H for (a) $(\phi/\phi_0)^2 = 0.015$ and (b) $(\phi/\phi_0)^2 = 0.74$.

when $(q, \eta) = (0.035, 0.8)$ and $(0.035, 0.8)$.) The measurements of p and $P^{(4)}$ were also performed as a function of Φ/ϕ for $(\phi/\phi_0)^2 = 0.005$ and $(\phi/\phi_0)^2 = 0.69$. It was found that for the small NA they start decreasing when Φ/ϕ exceeds unity, while for the large NA they are nearly constant regardless of Φ/ϕ. These results were also obtained with the single-longitudinal-mode operation of the argon-ion laser, indicating that the phase conjugation process of interest was less sensitive to the source temporal coherence.

The results shown above support the theoretical models given in [22], [23], [25], and [26], according to which nearly 50 percent of the reflected power which is not the power of the true phase-conjugate component but that of the depolarized component is distributed essentially uniformly over all the fiber modes, thus occupying ϕ_0 independently of ϕ. If the input beam occupies $\phi << \phi_0$ the full recovery of the true phase-conjugate signal is accomplished with an acceptance-beam diameter $\Phi = \phi$, resulting in a rejection of most of the noise power since only a small fraction $[(\phi/\phi_0)^2 << 1]$ of the noise power is contained within the NA occupied by the signal. This leads to high values (≥ 0.95) of p and $P^{(4)}$ with $\Phi/\phi \leq 1$. It also follows that under the above conditions as Φ/ϕ exceeds unity all the additional power reaching D_4 is due to the noise power, leading to decreases of p and $P^{(4)}$. If, on the other hand, the input-beam NA is increased until $\phi \approx \phi_0$ so that the input signal excites almost all of the fiber modes, the signal power per mode is reduced, while that of the noise remains the same, thus leading to a large R as well as to low constant values of p and $P^{(4)}$ that is almost independent of ϕ.

Fig. 10 shows photographs of the x-polarized phase conjugate images of the letter H when $(\phi/\phi_0)^2 = 0.015$ [Fig. 10(a)] and $(\phi/\phi_0)^2 = 0.74$ [Fig. 10(b)] [26]. As was discussed in the previous section, the degradation of the SNR is apparent from these two distinct photographs. Such degradation for large NA inputs was previously reported by Beckwith *et al.* [24].

IV. Applications

The image transmission and recovery in multimode fibers using phase conjugation, proposed by Yariv [43]–[45], may be the first application of a combination of multimode fibers and the PCM. In this case multimode fibers, in general, act not only as thick modal distorters but also as polarization scramblers. The experimental demonstrations of image recovery based on a round-trip propagation via phase conjugation were reported by employing nonpolarization-preserving PCM's (NPPPCM's) (which correspond to the present scheme) in the past [46]–[49]. The quality of image recovery was also discussed and compared to the case of the polarization-preserving PCM (PPPCM) [24]. It was found that for large NA inputs the resolution of the restored image is limited by the finite number of the fiber-guided modes independently of whether the PCM preserves polarization, and, as discussed in Section II, that the contrast is restored only when the PPPCM is used. The fiber-PCM combination has also been applied to fiber-optic interferometers/sensors [49]–[51] and gyros [31], [52]–[55]. Since these applications do not, in general, require large NA inputs, high-quality returned signals can be obtained with the NPPPCM's. Other applications of a combination of multimode fibers and the PCM reported so far are photorefractive oscillation with multimode fibers [53], [56] and optical interconnections [57]. The polarization-preserving property of the present scheme is also applicable to real-time image processing using wave polarization and phase conjugation [58].

In this section we describe six applications: 1) correction of nonreciprocal polarization distortions [27], 2) correction of lossy amplitude distortions [28], 3) phase-conjugate multimode fiber-optic interferometers [49], [50], 4) phase-conjugate multimode fiber-optic gyros [31], 5) temporal data channeling between beams [29], and 6) all-optical beam thresholding [30].

A. Correction of Nonreciprocal Polarization Distortions

The basic property of time reversal and distortion correction by phase conjugation breaks down if the propagation path includes nonreciprocal media such as magnetic (or gyrotropic) components. This follows mathematically from the fact that the presence of imaginary elements in the expressions for the magnetic susceptibility tensor spoils the invariance of Maxwell equations under complex conjugation for the reflected wave. To illustrate the effect, consider the case shown in Fig. 11(a), where a plane wave initially with complex transverse components $(\boldsymbol{E}_{x1}, \boldsymbol{E}_{y1})$ propagates through an element A, is phase conjugated, and returns to the initial plane after passing A in reverse. If the element A is a Faraday rotator with a Faraday angle θ, the round-trip is described by

$$\begin{pmatrix} E_x \\ E_y \end{pmatrix}_4 = \begin{pmatrix} \cos 2\theta & -\sin 2\theta \\ \sin 2\theta & \cos 2\theta \end{pmatrix} \begin{pmatrix} E_x^* \\ E_y^* \end{pmatrix}_1. \tag{45}$$

The vector $\boldsymbol{E}^{(4)}$ is thus *not* the complex conjugate of $\boldsymbol{E}^{(1)}$. (This can be compared to the case where the element A is dielectric (reciprocal), say, a retardation plate. Then the effect of the (reciprocal) retardation plate is canceled after a round-trip.)

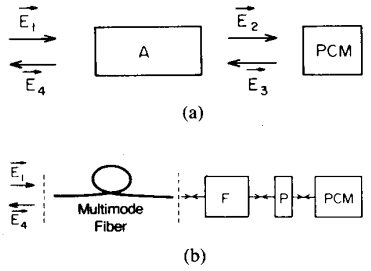

Fig. 11. (a) Schematic diagram of a wave that propagates through an element A, is phase conjugated, and returns to the initial plane. (b) A method to undo the nonreciprocal effect. P: polarizer; F: Faraday rotator.

In this subsection we describe a method [27] to undo the nonreciprocal effect on polarization by modal dispersal and phase conjugation [see Fig. 11(b)]. Assume a multimode fiber with a circular cross section. Adopting the same notations and procedure as those used in Section II but using a rotating coordinate (i.e., a circular polarization) representation, the phase-conjugate beam $\boldsymbol{E}^{(4)}$ can be written as

$$\boldsymbol{E}^{(4)} = rM'F'P'P^*F^*M^*(\boldsymbol{E}^{(1)})^* \tag{46}$$

where M and M' are the $2N$-rank scattering matrices of the fiber for the forward and the backward directions, P and P' are the matrices for the linear polarizer for the forward and the backward directions, and F and F' are the $2N$-rank Faraday rotation matrices for traveling along and opposite the magnetic field, respectively. For F and F' it is assumed that all of the fiber-guided modes $2N$ (N is the total number of the fiber-guided modes in one circular polarization) suffer the same amount of Faraday rotation θ. By using (46) together with the random coupling approximation used in Section II, it is found that

$$\boldsymbol{E}^{(4)} = \tfrac{1}{2}r \cos 2\theta(\boldsymbol{E}^{(1)})^* + \boldsymbol{U} \tag{47}$$

where $\boldsymbol{U}$, like $\boldsymbol{V}$ in (25), denotes the depolarized noise field. We note that (47) has the same form as (25) except for the factor $\cos 2\theta$.

From the same arguments as those described in obtaining (34) the polarized power P_{pol} and the depolarized noise power P_M can be expressed as

$$P_{\text{pol}} = 2\lambda \cos^2 2\theta \sum_{i=1}^{M} \Theta_i \tag{48a}$$

$$P_M = 2\lambda(2 - \cos^2 2\theta) \sum_{i=1}^{M} \Delta_i \tag{48b}$$

where λ is again given by $|r|^2 d/8$ and the effects of the residual polarization and of the quality of phase conjugation by the PCM are neglected (i.e., $q = 0$ and $\eta = 1$). From (48) the degree of polarization $P^{(4)}$ and the reflectivity R for the field $\boldsymbol{E}^{(4)}$ can be written as

$$P^{(4)} = \frac{\cos^2 2\theta}{(1 - \beta_2)\cos^2 2\theta + 2\beta_2} \simeq p \tag{49a}$$

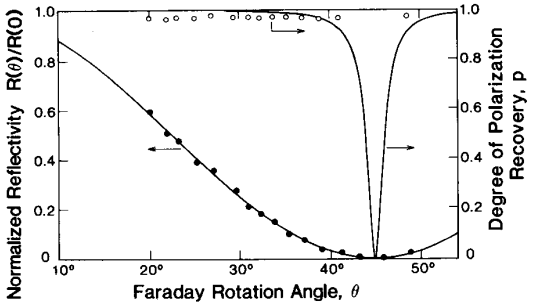

Fig. 12. Experimental results of the degree of polarization recovery p (○) and the normalized reflectivity $R(\theta)/R(0)$ (●). The solid lines are theoretical curves using a Gaussian noise distribution ($\psi/\phi_0 = 0.5$) and $(q, \eta) = (0, 1)$.

$$R(\theta) = \frac{1}{8}|r|^2 \sum_{i=1}^{M} \Theta_i[(2 - \beta_2)\cos^2 2\theta + 2\beta_2] \tag{49b}$$

where β_2 is defined by (36b). From (47) and (49) we notice that the polarization and spatial information of the field $\boldsymbol{E}^{(1)}$ can be recovered, provided that the input-beam NA is small (i.e., $\beta_2 \ll 1$) and that the Faraday rotation θ gives nonnegligible values of $\cos^2 2\theta$ compared to β_2 in (49).

The experiment was performed using the x-polarized input beam with the NA of 0.01. A variable Faraday rotator was used as the nonreciprocal media. The degree of the polarization recovery p and the x-polarized phase-conjugate power P_1 were measured. The experimental results are shown in Fig. 12, together with the theoretical curves of $P^{(4)}$ and $R(\theta)/R(0)$ calculated from (49). In the theoretical curves $\Sigma_{i=1}^{M} \Theta_i = 1$ and the Gaussian distribution of the noise intensity given by (39) with $(\phi/\phi_0)^2 = 0.001$ and $\psi/\phi = 0.5$ are used. It is seen that the normalized reflectivity $R(\theta)/R(0)$ varies almost as $\cos^2 2\theta$, while p is almost unity except in the vicinity of $\theta = 45°$. These theoretical curves are in good agreement with the experiment.

The above properties are applicable to a magnetic field sensor. In such a case a tandem combination of the Faraday medium F and the PCM act as the sensor part [59]. The magnetic field along the medium F induces Faraday rotations in the medium and can be detected by measuring the reflectivity R given by (49b). Because the detected signal is from the phase-conjugate wave of the input signal, self-aligned and stable operations can be expected.

To simulate distributed Faraday rotation in a fiber better, the theory was generalized to a sequence of N Faraday rotators separated by sections of fibers. The result, which was also proved experimentally with $N = 2$, simply replaces $\cos^2 2\theta$ in (49) by $\Pi_{i=1}^{N} \cos^2(2\theta_i)$. An experiment in which the magnetic field was directly applied along a fraction of the multimode fiber (about a 3 m part of the 20 m long fiber) was also conducted. It was observed that the degree of polarization recovery p is nearly unity in the range of 0 to 2 KG of the magnetic field, while the reflectivity R decreases monotonically with the increase of the

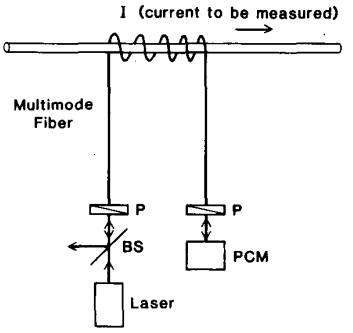

Fig. 13. Schematic diagram of a proposed current sensor. A beam from the laser propagates through a linear polarizer P and a multimode fiber. It is then reflected by the PCM and retraces its path.

magnetic field. It was found that (49b) replaced $\cos^2 2\theta$ by $\cos^{2N} 2\theta$ with $\theta = VHL/N$ (V is the Verdet constant of the fiber material, H the magnetic field, L the fiber length under the magnetic field) fit well with the experimental data when $N = 100$ was used. Although the reason for good agreement with $N = 100$ has not yet been clear and it should be the subject of the future study, the insensitivity of the polarization recovery to the magnetic field in this situation is an important factor for fiber-optic gyro applications [60]. The effect may also be used as a current sensor. In this case the current to be measured is enclosed by the multimode fiber coil (see Fig. 13). The current will be measured through the dependence of the reflectivity R on the magnetic field induced by the current. This proposed scheme is free from the problem of modal coupling that arises when a single-mode nonpolarization-preserving fiber is used for this purpose [61].

B. Correction of Lossy Amplitude Distortions

Most of the distortion correction schemes which are based on phase-conjugate optics involve phase distorting media [1]. This is due to the fact that distortion corrections cannot be achieved in cases involving inhomogeneous losses since part of the spatial information is lost and is not available for a reconstruction.

In this subsection we describe a method [28] of recovering an original image, including its polarization state, that has propagated through a lossy distorter by employing modal dispersal in a multimode fiber and a photorefractive PCM. In this method, before its incidence upon the lossy distorting medium, the image-bearing laser beam is intentionally mode dispersed by propagating through a (multi)mode- and polarization-scrambling fiber so that the field exiting the fiber has the original pictorial and polarization information spread among a large number of modes; this robustness enables it, within certain limits, to reconstruct the original field including the polarization. As mentioned earlier in this section, unlike the past studies of image transmission through multimode fibers [24], [43]–[49], the multimode fiber is used as a way to achieve mode and polarization scrambling of the input information in this study.

In the present paper the lossy distortion occurs between the fiber and the PCM in Fig. 1. Therefore the matrix C in (6), which accounts for the modal loss and mixing of the incoming field by the distortion, has the form of

$$C = \begin{pmatrix} C_{xx} & 0 \\ 0 & 0 \end{pmatrix} \tag{50}$$

where C_{xx} is an $N \times N$ submatrix which accounts for the elimination of the y-polarized field and the modal loss and mixing of the x-polarized field in the distorting medium. The form of the matrix C also implies that the loss does not scramble the polarizations. In particular we have $(C_{xx})_{ij} = \delta_{ij}$ when only a polarizer (oriented to the x direction) acts as the distorting medium [see (5)]. From (3) and (50) it is found that

$$M'CM^* = \begin{pmatrix} M'_{xx}C_{xx}M^*_{xx} & M'_{xx'}C_{xx}M^*_{xy} \\ M'_{yx}C_{xx}M^*_{xx} & M'_{yx}C_{xx}M^*_{xy} \end{pmatrix}. \tag{51}$$

In the case of a large number of nonvanishing elements $(C_{xx})_{ij}$ and using the random coupling approximation, each element in (51) can be approximated by

$$(M'CM^*)_{ij} \to \begin{cases} \dfrac{1}{2N}\sum_{k=1}^{N}(C_{xx})_{kk}, & \text{for } i = j \\ O(1/\sqrt{N}), & \text{for } i \neq j \end{cases}$$

where $M_{ij} = 1/\sqrt{2N}\exp(i\phi_{ij})$ is used, (see the Appendix B). It is therefore found that

$$\boldsymbol{E}^{(4)} = \frac{1}{2}r\left[\frac{1}{N}\sum_{k=1}^{N}(C_{xx})_{kk}\right](\boldsymbol{E}^{(1)})^* + \boldsymbol{W} \tag{52}$$

where $\boldsymbol{W}$ is a $2N$ rank vector whose elements depend on the elements of $\boldsymbol{E}^{(1)}$ and C_{xx} as well as N. We note that the first term on the right-hand side of (52) corresponds to the true phase-conjugate replica of the field $\boldsymbol{E}^{(1)}$ including its polarization state. The second term $\boldsymbol{W}$ corresponds to the (depolarized) noise. And as shown in Section II, in the absence of the lossy distorter (i.e., $(C_{xx})_{ij} = \delta_{ij}$) this noise contribution can be negligible in the limit where the input beam $\boldsymbol{E}^{(1)}$ excites, at the input, only a small fraction of the total number of modes $2N$ in the fiber, and the detection aperture is close to the input aperture so that only a small fraction of the noise power is included in the input aperture. In the present case it is seen from (52) that the true phase conjugation is possible, within the above limits, even when a large number of modes are lost by the distorting medium as long as the near equipartition of modal energy in the fiber is satisfied so that the input information is distributed equally among all of the modes.

In the experiment [28], a knife-edge F was used as the simulated amplitude distorter (or medium) in order to eliminate some portions of the input information. The input-beam NA was chosen to be about 0.036 that was much smaller than the fiber's NA of 0.29 so that the degradation of the phase conjugate signal due to the noise [corre-

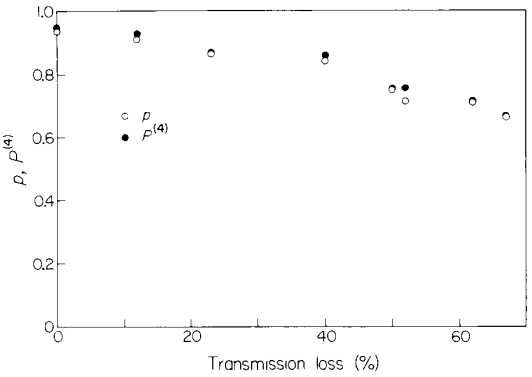

Fig. 14. The degree of polarization recovery p( ) and the degree of polarization $P^{(4)}$ (●) of the output field $E^{(4)}$ as a function of the transmission loss due to F for the linearly x-polarized input beam.

sponding to W in (52)] was negligible. The experimental setup was similar to Fig. 8 except that the out-coupled beam $E^{(2)}$ was either imaged onto F or quasi-collimated onto F, where a part of the beam was eliminated.

The degree of polarization recovery p and the degree of polarization $P^{(4)}$ of the field $E^{(4)}$ were first measured as a function of various transmission losses due to F, which is shown in Fig. 14. It is seen that p and $P^{(4)}$ are almost equal for all losses and both decrease as the loss increases. This shows that the original polarization recovery deteriorates gradually by the relative increase of the depolarized noise as the loss increases. This may indicate, as noted before, that the equipartition of the input information among all the modes in the fiber used is incomplete. Nonetheless the polarization recovery was still about 0.66, even in the case of the largest loss of 67 percent. Fig. 15 shows the results when the knife-edge F was placed at the image plane of the out-coupled field $E^{(2)}$. It is seen from Fig. 15(b) and (c) that the phase-conjugate image with F removed preserves its original polarization and spatial structure. It is also clear from Fig. 15(d)–(f) that although the intensities of the phase-conjugate images decrease as the transmission loss due to F increases, the phase-conjugate replica of the input image can be reconstructed. However, we see the apparent degradation of the spatial structure of the phase-conjugate image shown in Fig. 15(f). This may also be attributed, as mentioned above, to the incomplete equipartition of the input information among all the modes in the fiber. Therefore above a certain limit of the loss by F the reconstructed image bears less information than the original image, resulting in the apparent degradation. This effect may be analogous to the case of image reconstruction in holography with a diffused signal [62], when the resolution in the reconstructed image decreases as the fragment of hologram becomes smaller. In the present scheme the degradation depends strongly on the modal-scrambling nature in the fiber. The same results were also obtained when the knife edge F was placed at the quasi-collimated section of the field $E^{(2)}$. This fact indicates that, even if the mode scrambling of the input information in the fiber used is not complete, the input information is redistributed among a sufficiently large number of modes (viz., spatial frequencies) of the out-coupled field from the fiber and therefore the method is almost insensitive to the position of the distorter between the fiber and the PCM [63].

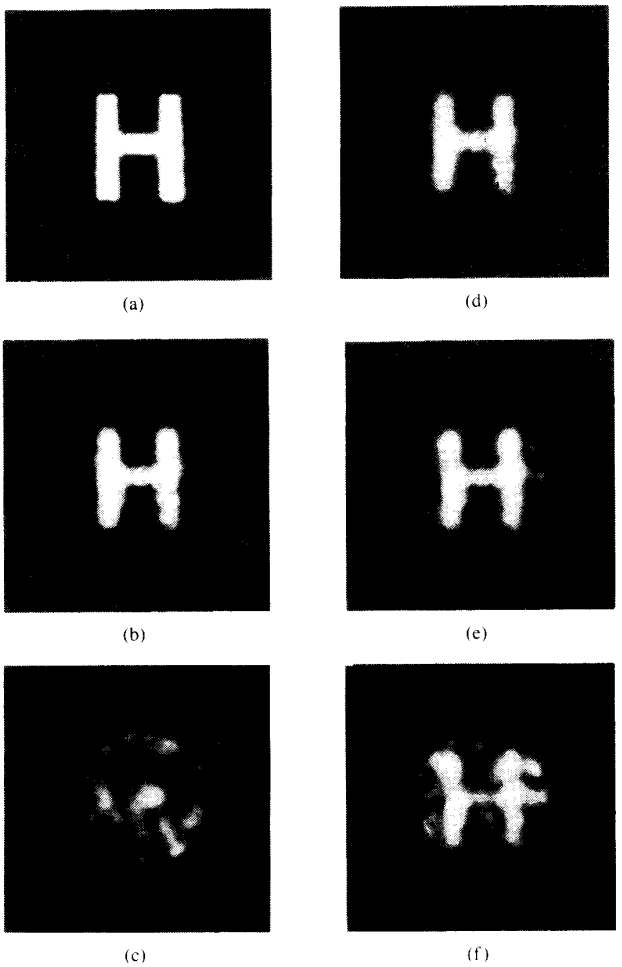

Fig. 15. (a) The x-polarized input image. (b) Phase-conjugate image of the x polarization without F (12 times the intensity-attenuated image). (c) Phase-conjugate image of the y polarization without F. (d)–(f) Phase-conjugate images of the x polarization with various transmission losses due to F; (d) loss 23 percent (12 times the intensity-attenuated image), (e) loss 53 percent (2 times the intensity-attenuated image), (f) loss 68.5 percent.

C. Phase-Conjugate Multimode Fiber-Optic Interferometers

Fiber-optic interferometers for sensing various physical purturbations (such as magnetic, acoustic, temperature, rotation) offer orders of magnitude increased sensitivity over existing technologies with remote-sensing capabilities and flexible interconnections within instruments [64]. In order to obtain stable operations, single-mode fibers have been used in the Mach–Zehnder-, Michelson-, and Fabry–Perot-type arrangements. On the other hand, multimode fibers have usually been employed as amplitude sensors, rather than as phase (interferometric) sensors,

with less sensitivities [64]. This is because coherent light suffers polarization scrambling and speckling during propagation in multimode fibers, as shown in Section II. However, because of several advantages over single-mode fibers such as ease of use, low cost and multichannel carrying capability, multimode fiber-optic interferometers for sensor applications are still favored and suggested [65], [66].

The use of the PCM's for multimode fiber-optic interferometers can suppress polarization-scrambling and speckling noise problems. In particular a self-pumped PCM with multimode fibers has been employed so far [49]–[51]. In a self-pumped PCM the pump beams $\boldsymbol{E}_1$ and $\boldsymbol{E}_2$ carry the same uniform phase as the input probe beam $\boldsymbol{E}_3$, since they are self-generated in a self-pumped PCM [14], [15]. Suppose a uniform phase change exp $(i\phi)$ of the input beam $\boldsymbol{E}_3$. According to the four-wave mixing process, the reflected conjugate beam $\boldsymbol{E}_4$ is proportional to $\boldsymbol{E}_1\boldsymbol{E}_2\boldsymbol{E}_3^*$ and the phase change of $\boldsymbol{E}_4$ is exp $(i\phi)$ exp $(i\phi)$ exp $(-i\phi)$ = exp $(i\phi)$, which is exactly the same as that of $\boldsymbol{E}_3$. Feinberg [67] experimentally demonstrated this property and also showed the correction capability of nonuniform phase distortions in the Michelson interferometer with a self-pumped PCM using internal reflection in one arm. The excellent linearity of this phase change as a function of the input uniform phase change and its instantaneous response property have also been confirmed recently by means of quantitative phase measurements [68]. Fischer and Sternklar [49] applied Feinberg's scheme to phase-conjugate interferometry with multimode fibers using a semilinear self-pumped PCM [15]. They obtained the interference-fringe pattern with high contrast. This scheme is shown in Fig. 16(a), where polarization scrambling and speckling of the field emitted from the fiber can be corrected in a double pass; yet the uniform phase change caused by some external perturbations to the fiber can be detected by the movement of the interference fringe. The problem of a frequency shift ($\leq$ a few Hz) of the conjugate beam relative to the input beam in a self-pumped PCM [69], [70] may be eliminated by introducing a frequency shift in the reference beam. This intentional frequency shift also enables us the heterodyne detection system used in usual fiber-optic interferometers [64]. Sternklar *et al.* [50] demonstrated the Mach–Zehnder interferometer with multimode fibers using the double phase-conjugate mirror (DPCM) [71]. This scheme is shown in Fig. 16(b). Because of the property of the DPCM a uniform phase change impressed on the beam propagating in the fiber is transferred to the other conjugate beam without any wavefront aberration [58], and the phase change can be detected by the fringe movement. Recently Kwong [51] has applied the scheme shown in Fig. 16(a) to a fiber-optic temperature sensor and obtained good correspondence between the temperature change at a small portion of the fiber and the fringe movement. These interferometers using multimode fibers and the self-pumped PCM and/or the DPCM give not only many advantages of multimode fibers over single-mode fibers but also high sensitivity and stability of the system.

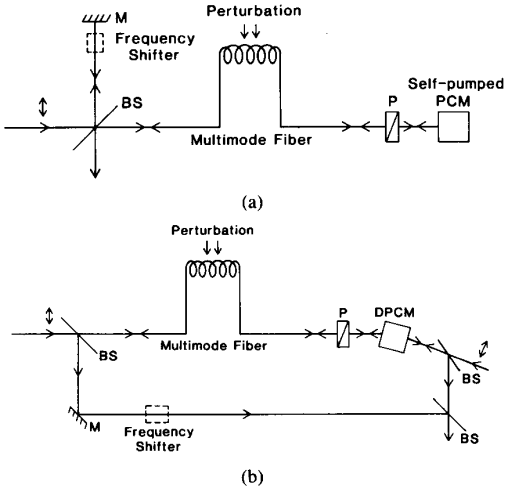

Fig. 16. Two configurations of phase-conjugate multimode fiber-optic interferometers: (a) Michelson interferometer; (b) Mach–Zehnder interferometer. Input beams are linearly polarized for both (a) and (b). Uniform phase changes of the input beams propagating in the fibers are impressed by some external perturbations such as temperature changes. Note that the frequency shifters illustrated in (a) and (b) are not essential, but are used for compensating the frequency shift of the conjugate beams relative to the input beams and/or for the heterodyne detection of the phase changes. P: polarizer; M: mirror; BS: beam splitter.

D. Phase-Conjugate Multimode Fiber-Optic Gyros

A fiber-optic gyro [60], [64] is one of the most important applications in fiber-optic sensor systems. Sagnac interferometers have usually been employed for this purpose because they are inherently insensitive to reciprocal phase shifts but are sensitive to nonreciprocal phase shifts [60], [64]. Multimode fiber-optic gyros have also been proposed [72], [73], but their sensitivity is limited by the modal scrambling in the fiber. For obtaining better sensitivity over some unwanted perturbations such as modal scrambling and Faraday effects, single-mode polarization-preserving fibers and couplers have been used [74].

Because time-reversed waves by phase conjugation can automatically correct reciprocal phase shifts but retain nonreciprocal ones during a round-trip propagation, the fiber-PCM combination can also be applied to a fiber-optic gyro. Moreover, by taking advantage of the polarization-preserving property of the present scheme for small NA inputs, multimode fibers may be employed. Fig. 17 shows a basic configuration of a phase-conjugate multimode fiber-optic gyro [31]. A linearly polarized beam is divided into two orthogonally polarized beams by PBS. The two beams are then launched into a multimode fiber coil and propagate clockwise and counterclockwise, respectively. After being emitted from the fiber coil ends, the two beams are phase conjugated by either the PPPCM (or the NPPPCM with a polarizer, not shown in the figure) and then propagate in the backward direction. In this

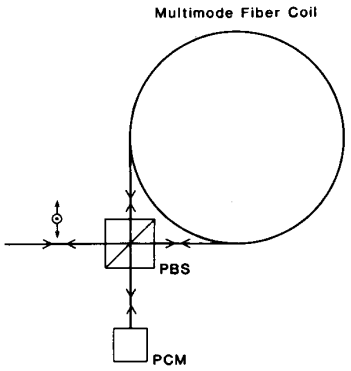

Fig. 17. Configuration of phase-conjugate multimode fiber-optic gyro. Input beam is linearly polarized at 45° to the plane of the figure. PBS: polarizing beam splitter; PCM: phase-conjugate mirror (PPPCM or NPPPCM).

case the phase difference ϕ between the recombining beams on the detection is given by [55]

$$\phi = \frac{8\pi RL\Omega}{\lambda c} \tag{53}$$

where R and L are the radius and length of the fiber coil, respectively, and Ω is the rotation rate, λ is the wavelength, and c is the speed of light. We note that, because of the round-trip propagation nature of phase conjugation, for given R and L the phase difference ϕ is 2 times larger than that in a conventional fiber-optic loop interferometer [60]. This new type of gyro using the multimode fiber-PCM configuration also has an advantage in that inexpensive and easy-to-use multimode fiber and couplers can be used, and that self-aligned coupling to the fiber can be obtained by phase conjugation.

The experimental proof-of-principle demonstrations of rotation sensing with phase-conjugate fiber-optic gyros were performed for the first time by using a Michelson interferometer with the externally pumped NPPPCM [54] and a Sagnac interferometer with the self-pumped PPPCM [55]. In both cases, however, single-mode polarization-preserving fibers were used. It should be noted that even for the latter case (i.e., the use of the self-pumped PCM) the nonreciprocal phase shift between two counter-propagating beams in the fiber can be detected since the relative phase change between the two input beams is truly reversed in a self-pumped PCM [55], [68]. Later, the multimode fiber and the self-pumped NPPPCM were employed for a Sagnac interferometer, and rotation sensing of 6°/s (which corresponds to the phase shift of 0.09 rad in that experiment) was demonstrated [31]. A different type of multimode fiber-optic gyro [53], using a photorefractive ring passive PCM [15] in which the ring consists of a multimode fiber, was previously reported.

In these phase-conjugate fiber-optic gyros the dynamic correction of reciprocal phase shifts is limited by the finite response time of phase conjugators [55], and changes in the phase-conjugate reflectivity of phase conjugators may be responsible for drift of output signals on a larger time scale [31]. In addition the depolarized fields in the reflected fields are one of the noise sources when a multimode fiber and the NPPPCM are employed [31]. Therefore the improvement of the system performance should be the subject of future studies.

E. Temporal Data Channeling Between Beams

Because of growing interest in photonic switching and interconnections [75], applications of nonlinear optical phase conjugation to signal processing in the temporal domain are also considerable. The functions proposed so far are: pulse envelope shaping, optical gating, time delay control, logic gating, convolution and correlation, envelope reversal, and space-to-time modulation–demodulation [1]. Recently, retromodulation–conjugation using a self-pumped PCM has also been reported [76].

In this subsection we describe a series of experiments [29] in which the input to the fiber-PCM combination consists of two separate optical beams, each with its own temporal modulation. It is found that, upon phase conjugation and reverse propagation through the fiber, almost-perfect recovery of the spatial and polarization properties of the beams is achieved with an exchange of temporal information between them.

The experimental setup is shown in Fig. 18. The input-beam NA of each beam was about 0.01, and the relative angle of incidence θ_i of the two beams on the fiber was ranged between 5 and 15°. The main results of the different experiments are summarized below.

1) Spatial Crosstalk: The two input beams were similarly polarized and run in the CW mode. If there is a considerable crosstalk between the two channels, it should manifest itself as a strong dependence of the reflectivity of each beam on the other beam's input power. Such a dependence was not found up to an input power ratio $P_2/P_1 = 10$. It should be emphasized that the spatial recovery was achieved in spite of the fact that only half of the incident modes (the horizontally polarized modes) were phase conjugated.

2) Polarization Recovery and Crosstalk: The degree of polarization recovery p_i

$$p_i = \frac{C_{ii} - C_{ij}}{C_{ii} + C_{ij}} \tag{54}$$

when C_{ii} and C_{ij} are the optical power of the two orthogonal polarization components reflected in the channel (i), was measured both when one beam is present and when two beams are coupled to the fiber, with different polarizations of the input beams. In all cases, it was found that in addition to the spatial recovery, there is no apparent crosstalk of polarization between the beams and a nearly complete polarization recovery is achieved.

3) Coupling of Temporal Structure: The temporal coupling of the two beams was investigated by a square wave modulating beam 2 at frequency f_2 while beam 1 was

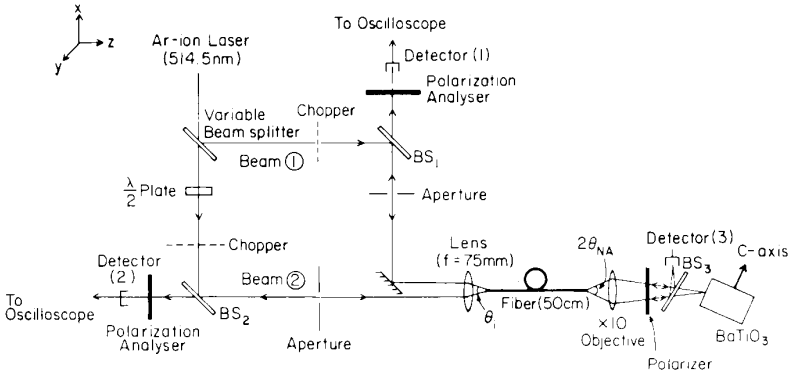

Fig. 18. Experimental arrangement for the two-beam coupling through the multimode fiber to the PCM.

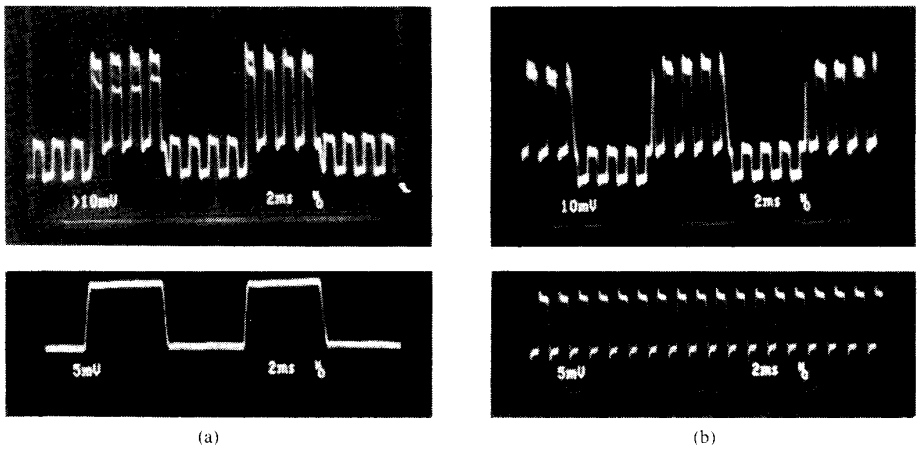

(a) (b)

Fig. 19. Picture of the input power (lower) and output power (upper) in case 2: (a) beam 2; (b) beam 1.

either constant (CW) (case 1) or modulated at a different frequency f_1 (case 2). The crystal parameters were such that the phase conjugation beam was a true replica of the input beam [77] without any phase difference of distortion when the modulation frequency ranged between 50 Hz to 1 kHz. Moreover, the reflectivity and rise time were also independent of f_2 in this range and were identical to those of a CW beam of the same average intensity.

In the first generic experiment designed to investigate temporal coupling beam 2 was modulated at f_2 while beam 1 was unmodulated. It was observed that the modulation format of beam 2 was grafted onto beam 1 and thereby both output beams were equally modulated. (See also Fig. 19.)

In a second experiment both beam 1 (f_1) and beam 2 (f_2) were modulated. The respective input and output beams are shown in Fig. 19. We notice that an exchange of the temporal information has taken place and, furthermore, that both output beams have similar envelopes. In addition, it was found that

1) the output beam's intensity ratio follows approximately the input ratio P_1/P_2,

2) full polarization and spatial recovery is achieved, and

3) the modulation index of each of the output beams is greater than that of the superposition of the input beams.

The last point is demonstrated by the graph in Fig. 20. It is seen that when $P_i/P_j \geq 3$, both output beams are almost completely modulated by f_1.

In what follows it is shown that a simple extension of the theoretical model presented in Section II to include temporal dependence of modes can be used to explain the qualitative nature of the observations mentioned above. The combined two-beam input field to the fiber can be expressed as

$$\boldsymbol{E}^{(1)} = \boldsymbol{E}_a^{(1)} + \boldsymbol{E}_b^{(1)} g(t) \tag{55}$$

where it is assumed that only beam b has a time-dependent factor $g(t)$. At the output of the fiber

$$\boldsymbol{E}^{(2)} = M\boldsymbol{E}^{(1)}. \tag{56}$$

Since only the x-polarized component of the field $\boldsymbol{E}^{(2)}$ is launched into the PCM (see Fig. 17), the field $\boldsymbol{E}_x^{(2)}$ is expressed as

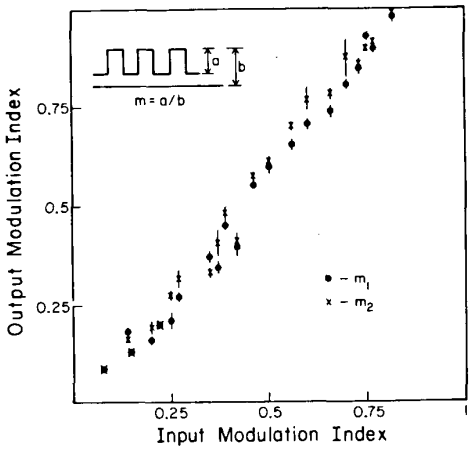

Fig. 20. A plot of the output modulation index of each of the beams in case 1 as a function of the combined beams input modulation index.

$$E_x^{(2)} \equiv (E_a^{(2)})_x + (E_b^{(2)})_x = \sum_{i=1}^{N} [v_{ai} + v_{bi} g(t)]. \tag{57}$$

For the phase-conjugation process in the crystal the model is simplified by considering one interaction region of the self-pumped PCM. The analogy between four-wave mixing and real-time holography [1] is invoked and it is assumed that each of the modes, say u_m, is reflected efficiently only by a grating which is created by two "writing" beams of the same mode. A "reference" beam $u_m^{(1)}$ and a "signal" beam $u_m^{(2)}$ create a "grating" $u_m^{(2)*} u_m^{(1)}$. A "reference" beam $u_m^{(3)} \propto u_m^{(1)*}(t)$ is scattered off the grating leading to phase-conjugated output beam:

$$u_m^{(4)} \propto \langle u_m^{(2)*} u_m^{(1)} \rangle u_m^{(1)*}(t) \tag{58}$$

where $\langle \cdots \rangle$ denotes time average. Since the response time of the photorefractive medium is too large to follow the field modulation $g(t)$ [15], the grating term $u_m^{(2)*} u_m^{(1)}$ is time-independent. The time dependence of $u_m^{(4)}$ is then dictated by that of the incident field $u_m^{(1)*}$ only.

Using the relation by (58) and keeping only the phase-matched terms in the scattering process by the grating, the phase-conjugate field $E^{(3)}$ is found to be

$$E^{(3)} = \sum_{i=1}^{N} [A_i(t) v_{ai}^* + B_i(t) v_{bi}^*] \tag{59}$$

where

$$A_i(t) = \rho_{a1} |v_{ai}|^2 + \rho_{a2} |v_{bi}|^2 + \rho_{a3} |v_{bi}|^2 g(t)$$

$$B_i(t) = \rho_{b1} |v_{ai}|^2 + \rho_{b2} |v_{bi}|^2 g(t) + \rho_{b3} |v_{bi}|^2 g(t)$$

in which ρ denotes the PCM modal reflectivity. From (56) and (57) we see that terms v_{ai} and v_{bi} contain the factors $m_{ij} \exp i\phi_{ij}$ of the scattering matrix elements. Therefore due to the random coupling approximation the main contributions of the terms $|v_{ai}|^2$, $|v_{bi}|^2$ and ρ in $A_i(t)$ and $B_i(t)$ are independent of the mode (i). Thus it is found that

$$E^{(3)} = A(t)(E_a^{(2)})_x^* + B(t)(E_b^{(2)})_x^*. \tag{60}$$

Using (56) and the same argument as those shown in Appendix B, the phase-conjugate field $E^{(4)}$ after the fiber is given by

$$E^{(4)} = A(t)(E_a^{(1)})^* + B(t)(E_b^{(1)})^* + X. \tag{61}$$

In the above equation X denotes the noise field that can be neglected for small NA inputs, thus proving the point of interest.

The temporal coupling phenomena shown above can be used to make, for example, a 1 to N optically interconnected switch, when $(N + 1)$ beams are interconnected together and one of them is carrying temporal information to be transferred to the others. Other applications, like optical time domain filters and signal processing, can also be considered.

F. All-Optical Beam Thresholding

The recent development of optical implementation of various data processing procedures has created a demand for a sensitive all-optical thresholding device [78], [79]. Several thresholding configurations using photorefractive crystals have been reported in the past [80]–[84]. In this subsection a possible mechanism for such a device [30] is presented, based on the coupling of mutually incoherent light beams by means of the fiber-coupled PCM.

In the experiment up to three mutually incoherent beams were converged into a multimode fiber with an incidence angle in the range of 0–10°. The rest of the experimental system was similar to that described in Section IV-E. It should be noted that, by launching all the input beams into one multimode fiber, the interaction between them in the crystal is maximized since the strong intermodal coupling in the multimode fiber makes the out-coupled beams almost independent of the initial characteristics of the input beams (i.e., angles of incidence, polarizations, and spatial structures) which are now distributed over all of the fiber-guided modes for each of the incident beams.

In the first set of experiments the phase-conjugate beams of two mutually-incoherent input beams were investigated. The steady-state phase-conjugate beam of each of the two beams (hereafter: $PC_1^{(0)}$ and $PC_2^{(0)}$) was first measured separately, and then the power of the steady-state phase-conjugate beam of each of the two beams (hereafter: PC_1 and PC_2) was measured while the two beams were coupled simultaneously to the fiber. It was found that only the stronger beam was phase conjugated, whereas the phase-conjugate light of the weaker beam was suppressed to zero.

In Fig. 21 the results of a measurement of PC_1 are shown as a function of the input-power difference $\Delta = P_1 - P_2$. It is seen that PC_1 depends on the input-power difference Δ, and not on P_1 alone. In Fig. 22 the another experimental result is shown, where instead of the self-pumped PCM with internal reflection [14] a ring passive PCM [15] was used. The resonator loss M in this PCM

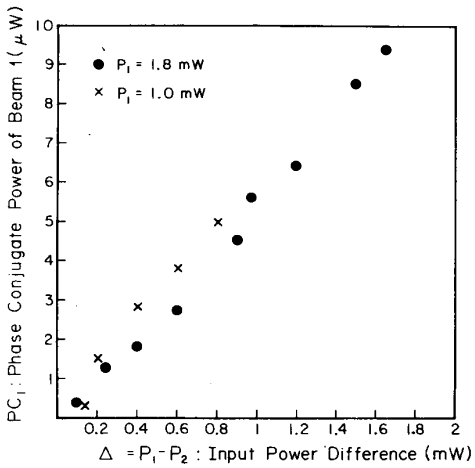

Fig. 21. Input power difference $\Delta = P_1 - P_2$ versus phase-conjugate power PC_1 of the beam 1.

was 0.65. Here the reflectivity of the signal beam is shown as a function of the normalized erasure beam power P_e/P_0 ($P_1 \equiv P_0$, $P_2 \equiv P_e$). Again we see the almost linear behavior of the reflectivity. We note, however, that the threshold power $P_e/P_0|_{\text{threshold}}$ depends on the signal power. This behavior can be explained by a simple phenomenological model [30], which is valid for signal input intensity less than $2\text{mW}/\text{mm}^2$. In this model the ring passive PCM under the incoherently erasing illumination upon the crystal is considered. The effective photorefractive coupling constant γ [30] is then given by

$$\gamma = \frac{\gamma_0}{1 + \dfrac{P_e}{P_0} + \dfrac{\sigma_d}{\sigma_p}} \tag{62}$$

where σ_d is the dark conductivity, σ_p the photoconductivity in the absence of P_e, and γ_0 the photorefractive coupling constant when $P_0 >> P_e$ and $\sigma_p >> \sigma_d$. Using (62) in the derivation of the phase-conjugate reflectivity of the ring passive PCM [15], it is found [30] that the experimental results shown in Fig. 22 can be explained qualitatively by the simple model. The calculated results are shown in Fig. 23, where $\gamma_0 l = 2.4$ (l is the interaction length in the crystal), $M = 0.65$ and $\sigma_d/\sigma_p = 0.5$ at $P_0 = 1.0$ mW are used. We see the same linear behavior of the reflectivity as that in Fig. 22 when P_0 takes the smaller values. This is because with the unsaturated gain γ_0 for the smaller value of P_0 the corresponding reflectivities are not saturated and small changes in γl cause nearly linear changes in the reflectivities. The reason for the normalized threshold power dependence on the signal power is that in the specific power the dark conductivity σ_d is still important and there is an implicit dependence of γ on P_0 through σ_p. As P_0 increases further, however, the theoretical curves tend to differ from the experimental results shown in Fig. 22 since the effects of multigratings become significant and the experimentally observed threshold values become greater than those predicted by the simple model.

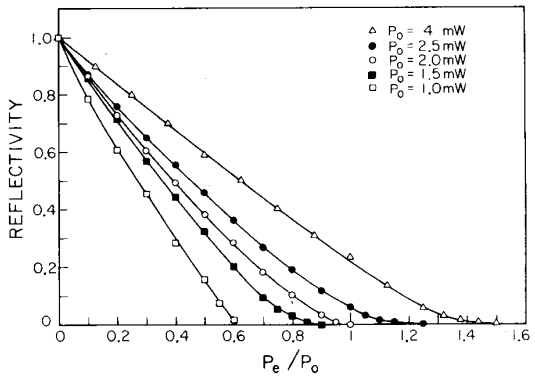

Fig. 22. Measured phase-conjugate reflectivity of the signal beam as a function of the normalized erasure beam power P_e/P_0 for several values of signal beam power P_0.

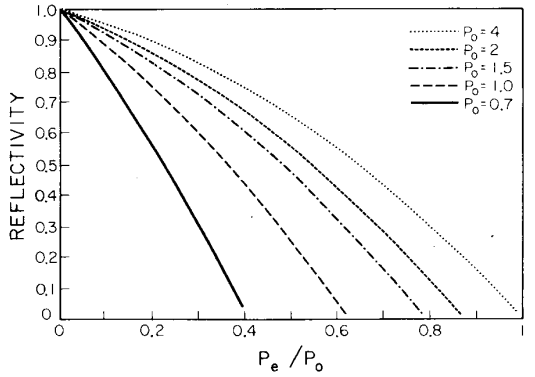

Fig. 23. Theoretical curves of the phase-conjugate reflectivity of the signal beam as a function of the normalized erasure beam power P_e/P_0 for several values of signal beam power P_0.

In the third set of experiments three mutually-incoherent beams were launched into the fiber-coupled PCM. Here the inputs of beams 2 and 3 were held fixed (with $P_2 > P_3$) and P_1 was varied. It was found here that as long as $P_1 > P_2 + P_3$, only beam 1 was phase conjugated. Moreover, in the intermediate range where none of the input beams were stronger than the sum of the two others, no phase-conjugate beam was emitted.

In all the above results, the phase-conjugate beams (above threshold) always show a good recovery of the original input information without crosstalk from the erasing beam, in accordance with the explanation given in the previous subsection. It should be noted that the thresholding is due to the input power ratio (not the intensity), and that each of the input beams can be regarded as either signal or erasure beams, making it possible to use the phenomena as all-optical beam thresholding and switching devices.

V. Conclusion

In this paper we have described the theoretical and experimental investigations of polarization and spatial information recovery by modal dispersal and phase conjugation. In the theoretical model two vital aspects have

been used: the modal dispersal of information and the modal averaging via phase conjugation. Because of these physical processes the initial information which is redistributed among all of the fiber modes can be recovered in spite of (partial) phase conjugation of only one field component of the mode-scrambled field emitted from the fiber. The depolarized noise associated with a reconstruction of the original information contains nearly the same amount of the total power as that of the reconstructed true phase-conjugate beam and is distributed among all of the fiber modes, independently of the mode distribution of the original input beam. Therefore the noise power per mode can be negligibly small compared to that of the true phase-conjugate beam when the input-beam NA is much smaller than the fiber's NA. This enables the complete recovery of polarization and spatial information. On the other hand, the fidelity of this true phase conjugation tends to degrade as the input-beam NA increases since the noise tends to intermingle with the reconstructed true phase-conjugate beam. Likewise, the SNR in a reconstructed image shows the similar effect of the depolarized noise on the SNR. The theory described in this paper has been found to be in good agreement with the experimental results. The concept of modal dispersal and phase conjugation has been applied to several novel applications: correction of nonreciprocal distortions, correction of lossy amplitude distortions, phase-conjugate multimode fiber-optic interferometers and gyros, temporal data channeling between beams, and all-optical beam thresholding. There is no doubt that, although the present scheme may be somewhat limited as far as pictorial information processing is concerned (i.e., when large NA inputs are required), it permits new signal processing applications involving sensors, gyroscopes, multichannel switching, and optical interconnections.

Appendix A
The Random Coupling Approximation

Each element of the scattering matrix M is expressed as

$$M_{ij} = m_{ij} \exp(i\phi_{ij}). \tag{A1}$$

The elements are interrelated by the unitarity condition given by (8) and (9). For the case of strong intermodal coupling in the fiber, the initially-excited fiber-guided modes at the input are redistributed among all of the fiber-guided modes during propagation. Then it is appropriate to assume that the amplitudes m_{ij} are either nearly the same or symmetrically and widely distributed with respect to the diagonal elements m_{ii}, while the phases ϕ_{ij} are distributed essentially uniformly over the $-\pi$ – $+\pi$ interval under the constraint of the unitarity condition. In this case the following *random coupling approximation* [26] may be adequate from (8) and (9):

$$\sum_{i=1}^{N} \left|(M_{kl})_{ij}\right|^2 \simeq \frac{1}{2} \tag{A2}$$

$$\sum_{j=1}^{N} \left|(M_{kl})_{ij}\right|^2 \simeq \frac{1}{2} \tag{A3}$$

where $k, l = x, y$ and $i, j = 1, \cdots, N$. In addition, due to the modal averaging over phase mismatched terms, all of the other cross terms are much smaller than unity for large N [21], [25].

Appendix B
The Qualitative Proof of Polarization and Spatial Information Recovery

In what follows, the qualitative proof [21], [25] of polarization and spatial information recovery is given by means of the random coupling approximation. As the simplest form of the scattering matrix M it is written as

$$M_{ij} = \frac{1}{\sqrt{2N}} \exp(i\phi_{ij}). \tag{B1}$$

Then the scattering matrix S in the round-trip propagation given by (22) can be expressed as

$$S \equiv M'CM^* = \begin{pmatrix} M'_{xx}M^*_{xx} & M'_{xx}M^*_{xy} \\ M'_{yx}M^*_{xx} & M'_{yx}M^*_{xy} \end{pmatrix} \tag{B2}$$

and

$$\begin{aligned}(M'_{xx}M^*_{xx})_{ij} &= (M'_{xx})_{ik}(M_{xx})^*_{kj} \\ &= (M_{xx})_{ki}(M_{xx})^*_{kj} \\ &= \frac{1}{2N}\sum_{k=1}^{N} \exp\left\{i\left[(\phi_{xx})_{ki} - (\phi_{xx})_{kj}\right]\right\} \\ &= \begin{cases} \frac{1}{2} & \text{for } i = j \\ O(1/\sqrt{N}) & \text{for } i \neq j \end{cases}\end{aligned} \tag{B3}$$

where summation over repeated indexes is made and (12) is used. The $N^{-1/2}$ in (B3) is due to the random-walk nature represented by the summation of the phasors $\exp \cdot \{i[(\phi_{xx})_{ki} - (\phi_{xx})_{kj}]\}$, independently of the fiber-guided modes that are excited initially [21], [25].

In a similar fashion it is found that

$$\begin{aligned}(M'_{yx}M^*_{xy})_{ij} &= \begin{cases} \frac{1}{2} & \text{for } i = j \\ O(1/\sqrt{N}) & \text{for } i \neq j \end{cases} \\ (M'_{xx}M^*_{xy})_{ij} &= O(1/\sqrt{N}) \\ (M'_{yx}M^*_{xx})_{ij} &= O(1/\sqrt{N}).\end{aligned} \tag{B4}$$

Then it is found that

$$S = S_1 + S_2$$

and

$$E^{(4)} = \tfrac{1}{2}r(E^{(1)})^* + V, \tag{B5}$$

where S_1 and S_2 correspond to (23), and V denotes the phase-mismatched noise field. We note that (B5) is equivalent to (25).

REFERENCES

[1] For reviews, see A. Yariv, "Phase conjugate optics and real-time holography," *IEEE J. Quantum Electron.*, vol. QE-14, pp. 650-660, 1978; also, *Optical Phase Conjugation*, R. A. Fisher, Ed. New York: Academic, 1983, and references therein.

[2] B. Ya. Zel'dovich and V. V. Shkunov, "Reversal of the wave front of light in the case of depolarized pumping," *Sov. Phys.—JETP*, vol. 48, pp. 214-219, 1978.

[3] V. N. Blashchuk, B. Ya. Zel'dovich, V. N. Krasheninnikov, N. A. Mel'nikov, N. F. Pilipetsky, V. V. Ragulsky, and V. V. Shkunov, "Stimulated scattering of depolarized radiation," *Sov. Phys.—Dokl.*, vol. 23, pp. 588-590, 1978.

[4] V. N. Blashchuk, V. N. Krasheninnikov, N. A. Mel'nikov, N. F. Pilipetsky, V. V. Ragulsky, V. V. Shkunov, and B. Ya. Zel'dovich, "SBS wave front reversal for the depolarized light—Theory and experiment," *Opt. Commun.*, vol. 27, pp. 137-141, 1978.

[5] N. G. Basov, V. F. Efimkov, I. G. Zubarev, A. V. Kotov, S. I. Mikhailov, and M. G. Smirnov, "Inversion of wavefront in SMBS of a depolarized pump," *Sov. Phys.—JETP Lett.*, vol. 28, pp. 197-201, 1978.

[6] B. Ya. Zel'dovich and V. V. Shkunov, "Spatial-polarization wavefront reversal in four-photon interaction," *Sov. J. Quantum Electron.*, vol. 9, pp. 379-381, 1979.

[7] B. Ya. Zel'dovich and T. V. Yakovleva, "Spatial-polarization wavefront reversal in stimulated scattering of the Rayleigh line wing," *Sov. J. Quantum Electron.*, vol. 10, pp. 501-505, 1980.

[8] In the past, spatial wavefront reversal of each of the two orthogonal polarizations having its own amplitude and phase (thereby incomplete spatial-polarization wavefront reversal) was found for depolarized pump waves in SBS [2]-[5]. An improved scheme which incorporates a two-plate tapered light guide prior to the SBS phase conjugator was recently reported for the complete reversal of depolarized pump waves. See I.D. Carr and D. C. Hanna, "Correction of polarization distortions using phase conjugation via stimulated Brillouin scattering," *Opt. Commun.*, vol. 52, pp. 396-402, 1987.

[9] V. N. Blashchuk, B. Ya. Zel'dovich, A. V. Mamaev, N. T. Pilipetsky, and V. V. Shkunov, "Complete wavefront reversal of depolarized radiation under degenerate four-photon interaction conditions (theory and experiment)," *Sov. J. Quantum Electron.*, vol. 10, pp. 356-358, 1980.

[10] G. Martin, L. K. Lam, and R. W. Hellwarth, "Generation of time-reversed replica of a nonuniformly polarized image-bearing optical beam," *Opt. Lett.*, vol. 5, pp. 185-187, 1980.

[11] J. Feinberg and R. W. Hellwarth, "cw Phase conjugation of a nonuniformly polarized optical beam," *J. Opt. Soc. Amer.*, vol. 70, p. 602, 1980.

[12] S. Saikan and M. Kiguchi, "Generation of phase-conjugated vector wave fronts in atomic vapors," *Opt. Lett.*, vol. 7, pp. 555-557, 1982.

[13] E. Ya. Korchemskaya, M. S. Soskin, and V. B. Taranenko, "Spatial polarization wavefront reversal under conditions of four-wave mixing in biochrome films," *Sov. J. Quantum Electron.*, vol. 17, pp. 450-454, 1987.

[14] J. Feinberg, "Self-pumped, continuous-wave phase conjugator using internal reflection," *Opt. Lett.*, vol. 7, pp. 486-488, 1982.

[15] M. Cronin-Golomb, B. Fischer, J. O. White, and A. Yariv, "Theory and applications of four-wave mixing in photorefractive media," *IEEE J. Quantum Electron.*, vol. QE-20, pp. 12-30, 1984.

[16] I. McMichael and M. Khoshnevisan, "Scalar phase conjugation using barium titanate crystal," in *Tech. Dig. Conf. Lasers and Electro-Opt.* Washington, DC: Opt. Soc. Amer., 1985, paper THN1, p. 220; I. McMichael, M. Khoshnevisan, and P. Yeh, "Polarization-preserving phase conjugator," *Opt. Lett.*, vol. 11, pp. 525-527, 1986.

[17] J. Feinberg, "Continuous-wave self-pumped phase conjugator with wide field of view," *Opt. Lett.*, vol. 8, pp. 480-482, 1983.

[18] P. Yeh, "Scalar phase conjugator for polarization correction," *Opt. Commun.*, vol. 51, pp. 195-197, 1984.

[19] K. Kyuma, A. Yariv, and S-K. Kwong, "Polarization recovery in phase conjugation by modal dispersal," *Appl. Phys. Lett.*, vol. 49, pp. 617-619, 1986.

[20] Y. Zhang, Y. Sun, X. Wang, and Z. Li, "Effect of optical phase conjugation on the polarization of the transmitted image field in a multimode fiber," in *Tech. Dig. Annu. Meet. Opt. Soc. Amer.* Washington, DC: Opt. Soc. Amer., 1986, paper FW8, p. 142.

[21] A. Yariv, Y. Tomita, and K. Kyuma, "Theoretical model for modal dispersal of polarization information and its recovery by phase conjugations," *Opt. Lett.*, vol. 11, pp. 809-811, 1986.

[22] R. Yahalom, Y. Tomita, and A. Yariv, "Effect of modal dispersal on the polarization and spatial information recovery in a fiber-coupled phase conjugate mirror," in *Postdeadline Papers of Conf. Lasers and Electro-Opt.* Washington, DC: Opt. Soc. Amer., 1987, paper THT6, p. 237; Y. Tomita, R. Yahalom, and A. Yariv, "Fidelity of polarization and spatial information recovery using a fiber-coupled phase conjugate mirror," *Opt. Lett.*, vol. 12, pp. 1017-1019, 1987.

[23] I. McMichael, P. Yeh, and P. Beckwith, "Correction of polarization and modal scrambling in multimode fibers by phase conjugation," *Opt. Lett.*, vol. 12, pp. 507-509, 1987.

[24] P. H. Beckwith, I. McMichael, and P. Yeh, "Image distortion in multimode fibers and restoration by polarization-preserving phase conjugation," *Opt. Lett.*, vol. 12, pp. 510-512, 1987.

[25] S. Wabnitz, "On the scattering matrix of multimode fibers for polarization recovery by phase conjugation," *J. Mod. Opt.*, vol. 34, pp. 1021-1024, 1987.

[26] Y. Tomita, R. Yahalom, and A. Yariv, "Theory of polarization and spatial information recovery by modal dispersal and phase conjugation," *J. Opt. Soc. Amer. B*, vol. 5, pp. 690-700, 1988.

[27] S-K. Kwong, R. Yahalom, K. Kyuma, and A. Yariv, "Optical phase-conjugate correction for propagation distortion in nonreciprocal media," *Opt. Lett.*, vol. 12, pp. 337-339, 1987.

[28] Y. Tomita, K. Kyuma, R. Yahalom, and A. Yariv, "Demonstration of correction of amplitude distortion by modal dispersal and phase conjugation," *Opt. Lett.*, vol. 12, pp. 1020-1022, 1987.

[29] R. Yahalom, K. Kyuma, and A. Yariv, "Phase conjugation of mode scrambled optical beams: Application to spatial recovery and inter-beam temporal information exchange," *Appl. Phys. Lett.*, vol. 50, pp. 792-794, 1987.

[30] R. Yahalom, A. Agranat, and A. Yariv, "Optical threshold mechanism using fiber coupled phase conjugate mirror," in *Tech. Dig. Top. Meet. Photonic Switching*, Lake Tahoe, Mar. 1987. Washington, DC: Opt. Soc. Amer., 1987, paper FB3; and also R. Yahalom and A. Yariv, "Optical thresholding using a fiber-coupled passive ring phase-conjugate mirror," *Opt. Lett.*, vol. 13, pp. 889-891, 1988.

[31] I. McMichael, P. Beckwith, and P. Yeh, "Phase-conjugate multimode fiber gyro," *Opt. Lett.*, vol. 12, pp. 1023-1025, 1987.

[32] K. Kim, L. Mandel, and E. Wolf, "Relationship between Jones and Mueller matrices for random media," *J. Opt. Soc. Amer. A*, vol. 4, pp. 433-437, 1987.

[33] A. Yariv, *Quantum Electronics*, 2nd ed. New York: Wiley, 1975, p. 357.

[34] S. Solimeno, B. Crosignani, and P. DiPorto, *Guiding, Diffraction, and Confinement of Optical Radiation*. New York: Academic, 1986, pp. 569-573.

[35] A. W. Snyder and J. D. Love, *Optical Waveguide Theory*. London, England: Chapman and Hall, 1983, p. 292.

[36] M. Born and E. Wolf, *Principles of Optics*, 5th ed. Elmsford, NY: Pergamon, 1975, pp. 544-555.

[37] See, for example, M. J. Stephen and G. Cwilich, "Rayleigh scattering and weak localization: Effects of polarization," *Phys. Rev. B*, vol. 34, pp. 7564-7572, 1986; K. A. O'Donnell and E. R. Mendez, "Experimental study of scattering from characterized random surfaces," *J. Opt. Soc. Amer. A*, vol. 4, pp. 1194-1205, 1987; M. B. Van der Mark, M. P. van Albada, and A. Lagendijk, "Light scattering in strongly scattering media: Multiple scattering and weak localization," *Phys. Rev. B*, vol. 37, pp. 3575-3592, 1988.

[38] For reviews, see Y. Nagaoka, Ed., "Anderson localization," Prog. Theor. Phys. Suppl., vol. 84, 1985; S. Chakravarty and A. Schmid, "Weak localization: The quasi-classical theory of electrons in a random potential," *Phys. Rep.*, vol. 140, pp. 193-236, 1986.

[39] Since the input-beam NA $\approx \phi/2f$ (f is a focal length of a lens) and M/N_{total} = (input-beam NA/fiber's NA)$^2/2$ (M = number of modes corresponding to ϕ for one polarization; $N_{\text{total}} = 2N$), we obtain $M/N_{\text{total}} = (\phi/\phi_0)^2/2$. In addition, since ϕ^2 is proportional to the solid angle Ω subtended by the beam launched into the fiber, then it also gives $(\phi/\phi_0)^2 = \Omega/\Omega_0$.

[40] J. W. Goodman, "Film-grain noise in wavefront-reconstruction imaging," *J. Opt. Soc. Amer.*, vol. 57, pp. 493-502, 1967.

[41] ——, "Statistical properties of laser speckle patterns," in *Laser Speckle and Related Phenomena*, 2nd ed. J. C. Dainty, Ed. Berlin, West Germany: Springer-Verlag, 1984, pp. 9-75.

[42] In practice, however, the use of the analyzer may improve the SNR better than that in the calculation because of the rejection of unwanted noise due to the back reflection from optical components.

[43] A. Yariv, "Three-dimensional pictorial transmission in optical fibers," *Appl. Phys. Lett.*, vol. 28, pp. 88-89, 1976.

[44] A. Yariv, "On transmission and recovery of three-dimensional image information in optical fibers," *J. Opt. Soc. Amer.*, vol. 66, pp. 301-306, 1976.
[45] A. Gover, C. P. Lee, and A. Yariv, "Direct transmission of pictorial information in multimode optical fibers," *J. Opt. Soc. Amer.*, vol. 66, pp. 306-311, 1976.
[46] V. V. Ivakhnik, V. M. Petnikova, M. S. Solomatin, and V. V. Shuvalov, "Compensation of wavefront distortions in a thick inhomogeneous medium," *Sov. J. Quantum Electron.*, vol. 10, pp. 373-375, 1980.
[47] G. J. Dunning and R. C. Lind, "Demonstration of image transmission through fibers by optical phase conjugation," *Opt. Lett.*, vol. 7, pp. 558-560, 1982.
[48] B. Fischer and D. Peri, "Real-time three-dimensional imaging through fiber bundles by four-wave mixing," *Opt. Lett.*, vol. 10, pp. 182-183, 1985.
[49] B. Fischer and S. Sternklar, "Image transmission and interferometry with multimode fibers using self-pumped phase conjugation," *Appl. Phys. Lett.*, vol. 46, pp. 113-114, 1985.
[50] S. Sternklar, S. Weiss, M. Segev, and B. Fischer, "Mach-Zehnder interferometer with multimode fibers using the double phase-conjugate mirror," *Appl. Opt.*, vol. 25, pp. 4518-4520, 1986.
[51] N. S.-K. Kwong, "A novel scheme for fiber optic sensors using a tandem combination of a multimode fiber and a self-pumped phase conjugator," in *Postdeadline Papers Conf. Optical Fiber Sensors*. Washington, DC: Opt. Soc. Amer., 1988.
[52] C. J. Bode, "Phase conjugate optics and applications to interferometry and to laser gyros," in *Experimental Gravitation and Measurement Theory*, P. Meystre and M. O. Scully, Eds. New York: Plenum, 1983, pp. 269-291.
[53] B. Fischer and S. Sternklar, "New optical gyroscope based on the ring passive phase conjugator," *Appl. Phys. Lett.*, vol. 47, pp. 1-3, 1985.
[54] P. Yeh, I. McMichael, and M. Khoshnevisan, "Phase-conjugate fiber-optic gyro," *Appl. Opt.*, vol. 25, pp. 1029-1030, 1986.
[55] I. McMichael and P. Yeh, "Self-pumped phase-conjugate fiber-optic gyro," *Opt. Lett.*, vol. 11, pp. 686-688, 1986.
[56] B. Fischer, S. Sternklar, and S. Weiss, "Photorefractive oscillation with intracavity image and multimode fiber," *Appl. Phys. Lett.*, vol. 48, pp. 1567-1569, 1986.
[57] H. J. Caulfield, J. Shamir, and Q. He, "Flexible two-way optical interconnections in layered computers," *Appl. Opt.*, vol. 26, pp. 2291-2292, 1987.
[58] Y. Tomita, R. Yahalom, and A. Yariv, "Real-time image subtraction using wave polarization and phase conjugation," *Appl. Phys. Lett.*, vol. 52, pp. 425-427, 1988.
[59] A magnetic field sensor using a single-mode polarization-preserving fiber and a normal mirror has also been proposed by A. Enokihara, M. Izutsu, and T. Sueta, "Optical fiber sensors using the method of polarization-rotated reflection," *J. Lightwave Technol.*, vol. LT-5, pp. 1584-1590, 1987.
[60] R. A. Bergh, H. C. Lefevre, and H. J. Shaw, "An overview of fiber-optic gyroscopes," *J. Lightwave Technol.*, vol. LT-2, pp. 91-107, 1984.
[61] A. Yariv, "Operator algebra for propagation problems involving phase conjugation and nonreciprocal elements," *Appl. Opt.*, vol. 26, pp. 4538-4540, 1987.
[62] R. J. Collier, C. B. Burckhardt, and L. H. Lin, *Optical Holography*. New York: Academic, 1971, p. 197.
[63] It should be noted that since the experiment is made for the distorter placed on both the image plane and the far-field plane of the fiber end, the phase-conjugate images obtained here *are not* a consequence of simple Fourier filtering of the input image.
[64] T. G. Giallorenzi, J. A. Bucaro, A. Dandridge, G. H. Sigel, Jr., J. H. Cole, S. C. Rashleigh, and R. G. Priest, "Optical fiber sensor technology," *IEEE J. Quantum Electron.*, vol. QE-18, pp. 626-665, 1982.
[65] M. R. Layton and J. A. Bucaro, "Optical fiber acoustic sensor utilizing mode-mode interference," *Appl. Opt.*, vol. 18, pp. 666-670, 1979.
[66] M. Imai, T. Ohashi, and Y. Ohtsuka, "Multimode-optical-fiber Michelson interferometer," *J. Lightwave Technol.*, vol. LT-1, pp. 75-81, 1983.
[67] J. Feinberg, "Interferometer with a self-pumped phase-conjugating mirror," *Opt. Lett.*, vol. 8, pp. 569-571, 1983.
[68] Y. Tomita, R. Yahalom, and A. Yariv, "On phase shift of a self-pumped phase-conjugate mirror," in Tech. Dig. Annu. Meet. Opt. Soc. Amer. Washington, DC: Opt. Soc. Amer., 1988, paper FB8, p. 161; and also submitted for publication.
[69] W. B. Whitten and J. M. Ramsey, "Self-scanning of a dye laser due to feedback from a $BaTiO_3$ phase-conjugate reflector," *Opt. Lett.*, vol. 9, pp. 44-46, 1984.
[70] J. Feinberg and G. D. Bacher, "Self-scanning of a continuous-wave dye laser having a phase-conjugating resonator cavity," *Opt. Lett.*, vol. 9, pp. 420-422, 1984.
[71] S. Weiss, S. Sternklar, and B. Fischer, "Double phase-conjugate mirror: Analysis, demonstration and application," *Opt. Lett.*, vol. 12, pp. 114-116, 1987.
[72] G. A. Pavlath and H. J. Shaw, "Multimode fiber gyroscopes," in *Fiber-Optic Rotation Sensors*, S. Ezekial and H. Arditty, Eds. Berlin, West Germany: Springer-Verlag, 1982, pp. 111-114.
[73] S. V. Bessonova, A. A. Borodkin, A. G. Dobrolynbova, E. V. Polyakov, V. P. Sarantev, A. T. Semenov, and V. A. Simakov, "Fiber-optic ring interferometer with a multimode waveguide," *Sov. J. Quantum Electron.*, vol. 13, pp. 1403-1405, 1983.
[74] W. K. Burns, R. P. Moeller, C. A. Villarnel, and M. Abebe, "All-fiber gyroscope with polarization-holding fiber," *Opt. Lett.*, vol. 9, pp. 570-572, 1984.
[75] For example, *IEEE Trans. Commun.*, Special Issue on Photonic Switching, vol. COM-25, Mar. 1987; A. A. Sawchuk, B. K. Jenkins, C. S. Raghavendra, and V. Varma, "Optical crossbar networks," *IEEE Trans. Comput.*, vol. C-36, pp. 50-60, June 1987.
[76] D. M. Pepper, "Hybrid phase conjugator/modulators using self-pumped 0°-cut and 45°-cut $BaTiO_3$ crystals," *Appl. Phys. Lett.*, vol. 49, pp. 1001-1003, 1986.
[77] B. R. Suydam and R. A. Fisher, "Transient response of Kerr-like phase conjugators: A review," *Opt. Eng.*, vol. 21, pp. 184-189, 1982.
[78] A. Yariv, S.-K. Kwong, and K. Kyuma, "Demonstration of an all-optical associative holographic memory," *Appl. Phys. Lett.*, vol. 48, pp. 1114-1116, 1986.
[79] B. H. Soffer, G. J. Dunning, Y. Owechko, and E. Marom, "Associative holographic memory with feedback using phase-conjugate mirrors," *Opt. Lett.*, vol. 11, pp. 118-120, 1986.
[80] M. B. Klein, G. J. Dunning, G. C. Valley, R. C. Lind, and T. R. O'Meara, "Imaging threshold detector using a phase-conjugate resonator in $BaTiO_3$," *Opt. Lett.*, vol. 11, pp. 575-577, 1986.
[81] S.-K. Kwong, M. Cronin-Golomb, and A. Yariv, "Optical bistability and hysteresis with a photorefractive self-pumped phase-conjugate mirror," *Appl. Phys. Lett.*, vol. 45, pp. 1016-1018, 1984.
[82] S.-K. Kwong and A. Yariv, "Bistable oscillations with a self-pumped phase-conjugate mirror," *Opt. Lett.*, vol. 11, pp. 377-379, 1986.
[83] M. Cronin-Golomb and A. Yariv, "Semi-self-pumped phase-conjugate mirrors," *Opt. Lett.*, vol. 12, pp. 714-716, 1987.
[84] S. Sternklar, S. Weiss, and B. Fischer, "Optical information processing with the double phase-conjugate mirror," *Opt. Eng.*, vol. 26, pp. 423-427, 1987.

Yasuo Tomita (S'88-M'89) was born in Sapporo, Japan, on September 28, 1955. He received the B.E. and M.E. degrees, both in electronic engineering, from Hokkaido University, Sapporo, Japan, in 1978 and 1980, respectively, and the M.S. degree in electrical engineering from the California Institute of Technology, Pasadena, in 1985. During his graduate study at the Research Institute of Applied Electricity, Hokkaido University, he investigated the statistical properties of white light and polychromatic speckles.

In 1980 he joined the Canon Research Center, Tokyo, Japan, where he worked on magnetooptics and its applications to erasable optical memories. In 1982-1983 he was a Visiting Associate at the Institute of Industrial Science, University of Tokyo, Tokyo. Since 1984 he has been with Caltech on leave from the Canon Research Center. He is now a Ph.D. candidate in electrical engineering at Caltech. His current research interests include propagation characteristics of conjugate waves in strongly scattering media and their applications, photorefractive nonlinear optics, nonlinear optical phenomena in passive and active waveguides, and optical computing. He has published many papers in the areas of speckles, magnetooptics, and phase conjugation.

Mr. Tomita is a member of the Japan Society of Applied Physics, the Optical Society of America, and the American Physical Society.

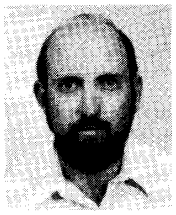

Ram Yahalom was born in Israel in 1952. He received the B.Sc. and Ph.D. degrees in physics from the Technion—Israel Institute of Technology, Haifa, in 1974 and 1984, respectively.

From 1974 to 1979 he served in the Israeli Defence Forces and was also involved in the research and development of electrooptic systems. After receiving the Ph.D. degree he spent one year as a research associate at the Stanford University, Stanford, CA, when he was awarded the Rothschild Fellowship. Since 1986 he has been a research fellow at the California Institute of Technology. His research interests include nonlinear optics and phase conjugation.

Kazuo Kyuma (M'87) was born in Tokyo, Japan, on October 22, 1949. He received the B.S., M.S., and Ph.D. degrees, all in electronic engineering, from the Tokyo Institute of Technology, Tokyo, Japan, in 1972, 1974, and 1977, respectively. At the Tokyo Institute of Technology, his studies were primarily in the field of the fabrication techniques of ZnO-sputtered films and their applications to the surface acoustic wave devices with semiconductor substrates.

In 1977, he joined the Central Research Laboratory, Mitsubishi Electric Corporation, Hyogo Prefecture, Japan. After that, he extended his speciality to optical devices. His recent research interests cover fiber-optic sensors including optical gyroscopes, integrated semiconductor lasers, optical switching devices, optical phase conjugation, and optical neural computers. From 1985 to 1986, he was a Visiting Associate at California Institute of Technology, Pasadena, CA, in the laboratory of Dr. A. Yariv. He has been the Manager of Photonics Group 1, Department of Advanced Device Technology, since 1987.

Dr. Kyuma is a member of the International Neural Network Society, the Institute of Electronics and Communication Engineers of Japan, the Japan Society of Applied Physics, and the Society of Instrument and Control Engineers.

Amnon Yariv (S'56-M'59-F'70), a native of Israel, obtained the B.S., M.S., and Ph.D. degrees in electrical engineering from the University of California, Berkeley, in 1954, 1956, and 1958, respectively.

He joined Bell Telephone Laboratories, Murray Hill, NJ, in 1959, at the early stages of the laser effort. He came to the California Institute of Technology, Pasadena, in 1964 as an Associate Professor of Electrical Engineering, becoming a Professor in 1966. In 1980 he became the Thomas G. Myers Professor of Electrical Engineering and Applied Physics. On the technical side, he took part (with various co-workers) in the discovery of a number of early solid-state laser systems, in proposing and demonstrating semiconductor based integrated optics technology, and in pioneering the field of phase conjugate optics. His present research efforts are in the areas of nonlinear optics, semiconductor lasers, and integrated optics. He has published widely in the laser and optics fields some 300 papers and has written a number of basic texts in quantum electronics, optics, and quantum mechanics. He is also a founder and chairman-of-the-board of the Ortel Corp., Alhambra, CA.

Dr. Yariv is a member of the American Physical Society, Phi Beta Kappa, the American Academy of Arts and Sciences, and the National Academy of Engineering, and a Fellow of the Optical Society of America. He received the 1980 Quantum Electronics Award of the IEEE, the 1985 University of Pennsylvania Pender Award, and the 1986 Optical Society of America Ives Medal.

Norman Sze-Keung Kwong (M'87) was born in Hong Kong on August 5, 1958. He received the B.Sc. degree in physics from the University of Hong Kong in 1980, the M.S. degree in physics from the University of Southern California, Los Angeles, in 1981, and the Ph.D. degree in physics from the California Institute of Technology, Pasadena, in 1986. As an undergraduate, he conducted experiments on measuring cosmic ray muon intensity. His doctoral work at Caltech concerned two-wave and four-wave mixing, phase conjugation, image processing, associative memories, and bistabilities with photorefractive materials.

Since 1986, he has been a Staff Scientist at the Ortel Corp., Alhambra, CA, where he continues his research on image processing and optical fiber sensors using photorefractive materials. He also manages a program to develop high-power GaAlAs and InGaAsP superluminescent diodes.